Supporting Information

Silver Nanoparticles: Facile Synthesis and their Catalytic Application for the degradation of dyes

Kamaldeep Sharma,‡ Gurpreet Singh,‡ Gurpreet Singh,‡ Manoj Kumar and Vandana Bhalla*

Department of Chemistry, UGC Centre for Advanced Studies-I, Guru Nanak Dev University, Amritsar, Punjab-143005- INDIA

vanmanan@yahoo.co.in

Contents

S17 XRD diffraction patterns of AgNPs of derivative **5** and **7.**

S18 Cyclic voltammograms and Onsets of Cathodic peaks and Cathodic peak potentials of $AgNO_3$ and derivatives **3**, **5** and **7** in the presence of $AgNO_3$ in H_2O/ACN (1/9, v/v) mixture.

S19 UV–visible spectra of derivative **5** (10 μm) upon addition of Ag^+ ions (200 equiv.) at different time intervals in H_2O/THF and graphical representation of the rate of formation of AgNPs of derivative **5** in the presence of KI**.**

S20-S21 Degradation of methylene blue, methyl orange and eriochrome black T over time using *in-situ* generated AgNPs by derivative **3** as catalyst in the presence of $NaBH_4$.

S22-S25 Degradation of Rhodamine B, methyl orange, methylene blue and eriochrome black T over time using *in-situ* generated AgNPs by derivative **5** as catalyst in the presence of $NaBH_4$.

S26-S29 Degradation of methyl orange, methylene blue, Rhodamine B and eriochrome black T over time using *in-situ* generated AgNPs by derivative **7** as catalyst in the presence of $NaBH_4$.

S30 UV-vis spectral changes of RhB over time using derivative **3**-stabilized AgNPs as catalyst under visible light irradiations in the presence of triethanolamine (TEOA).

S31-S32 Derivatives **3**, **5** and **7** stabilized AgNPs catalyst-reusing experiments.

S33 Blank experiment for the degradation of Rhodamine B, methylene blue, methyl orange and eriochrome black T.

S34 ^1H NMR spectrum of derivative **3**.

S35 Mass spectrum of derivative **3**.

S36 ^1H NMR spectrum of derivative **5**.

S37 ^{13}C NMR spectrum of derivative **5**.

S38 Mass spectrum of derivative **5**.

S39 ^1H NMR spectrum of derivative **7**.

S40 ^{13}C NMR spectrum of derivative **7**.

S41 Mass spectrum of derivative **7**.

Table S1: Comparison of this method in present manuscript over other reported procedure in literature for the preparation of AgNPs.

Method of formation of AgNPs	**Reducing agent or surfactant**	**Reaction temp.**	**Journals**
Wet chemical route	**No**	**Room temp.**	**Present manuscript**
Chemical method	Trisodium citrate	90 ^{0}C	*Chem. Mater.*,**2014**, *26*, 2836−2845
Chemical method	Sodium borohydride	-	*Journal of Materials*, **2014**, *2*, 6850-6858
Chemical method	poly(acrylic acid) (PAA)	~ 25 ^{0}C	*Chem. Mater.*,**2014**, *26*, 1332−1339
Chemical method	$NaBH_4$ Trisodium citrate	60 ^{0}C 90 ^{0}C	*RSC Adv*., **2014**, *4*, 3974–3983.
Chemical method	NaOH	Room temp.	*New J. Chem.*, **2014**, *38*, 2847-2855
Microwave Heating Method	Sodium laurate (Lau)	Microwave Heating	*Angew. Chem. Int. Ed.*, **2013**, *52*, 7446–7450
Chemical method	$NaBH_4$	Room temp.	*ACS Appl. Mater. Interfaces*, **2013**, *5*, 646−653
Chemical method	Polyvinylpyrrolidone (PVP)	140 ^{0}C	*Langmuir*, **2012**, *28*, 8845−8861
Photomediated methods	Trisodium citrate	Irradiated at 150 W halogen lamp	*Nano Lett*. **2011**, *11*, 2495–2498
Photomediated methods	$NaBH_4$	4 ^{0}C	*J. Am. Chem. Soc.*, **2010**, *132*, 12502–12510

Table S2: Comparison of present method for the degradation of Rhodamine B by *in-situ* generated AgNPs of derivative **3** over silver based reported systems in literature.

Reaction time for degradation of RB	**Catalyst used**	**Rate constants**	**Amount of catalyst used**	**Journals**
2.5 min.	**AgNPs**	**1.47 min^{-1}** **(2.44×10^{-2} sec^{-1})**	**3 µl**	**Present Manuscript**
30 min.	Citrate-coated AgNPs	0.064 min^{-1} (1.06×10^{-3} sec^{-1})	50 µl	Chem. Mater., 2014, 26, 2836-2844
14 min.	Ag-coated ZnO NWs	0.11 min^{-1} (1.83×10^{-3} sec^{-1})	-	J. Mater.Chem. C,2009,19,5547 5553
5 min.	Ag-graphene oxide NCs	0.38 min^{-1} (6.33×10^{-3} sec^{-1})	-	J. Hazard. Mater., 263P (2013) 5260
7 min.	AgI@TiO_2 nanoparticles	0.44 min^{-1} (7.33×10^{-3} sec^{-1})	10 mg	Dalton Trans., 2013, 42, 8796–8801
150 min.	Ag@TiO_2	0.02029 min^{-1} (3.38×10^{-4} sec^{-1})	80 mg	*CrystEngComm*, 2014, 16, 2384 2394
120 min.	Ag:ZnO nanostructures photocatalysts	100×10^{-4} min^{-1} (1.67×10^{-4} sec^{-1})	30 ml	*Appl. Phys. A*, (2012) 107:401–410
4 min.	Fe_3O_4@SiO_2@AgCl : Ag nanocomposites	1.015 min^{-1} (1.69×10^{-2} sec^{-1})	5 ml	*J. Mater. Chem.*, 2012, 22, 5171–5176

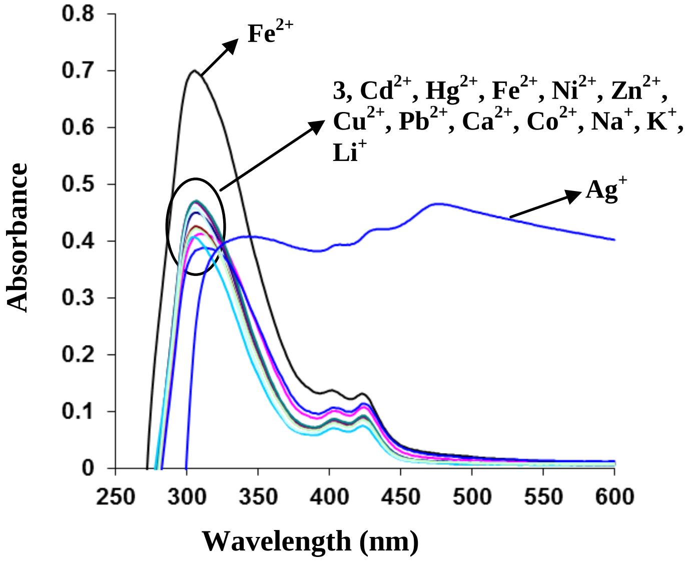

Fig. S1 UV-vis spectra of derivative **3** (10 μM) upon additions of 100 equivalents of various metal ions as their perchlorate salt in H_2O/THF (9.5/0.5), buffered with HEPES, pH = 7.0.Same equivalents of aqueous solution of $AgNO_3$ was used in case of Ag^+ metal ion.

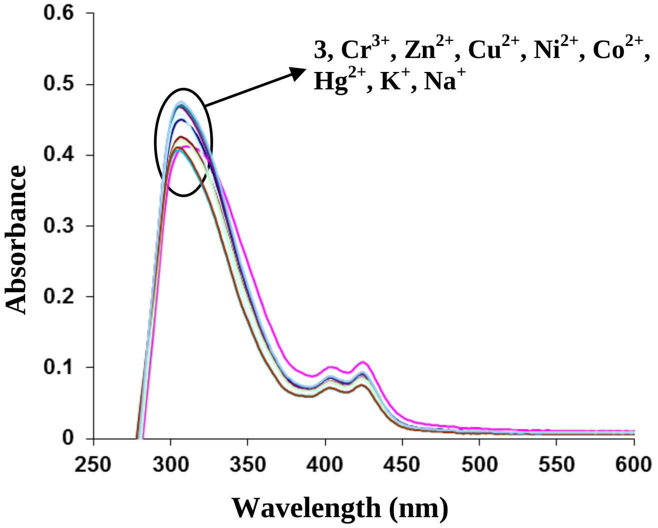

Fig. S2 UV-vis spectra of derivative **3** (10 μM) upon additions of 100 equivalents of various metal ions as their chloride salt in H_2O/THF (9.5/0.5), buffered with HEPES, pH = 7.0.

Regression Statistics	
Multiple R	0.95661
R Square	0.915102
Intercept	0.1636
Slope	0.129943

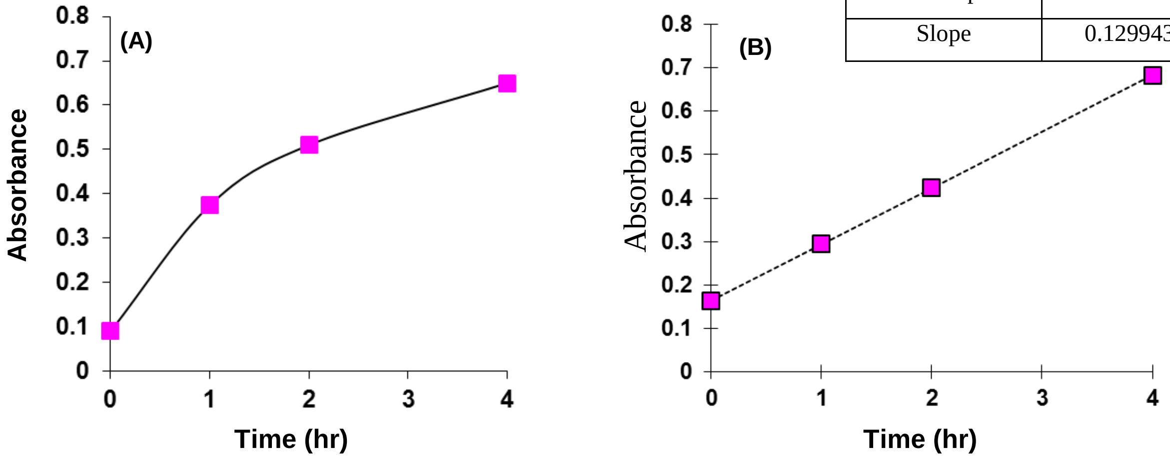

Fig. S3 Graphical representation of the rate of formation of AgNPs of derivative **3**. (A) Time (min.) vs. absorbance plot at 470 nm (B) regression plot of A.

The first order[1] rate constant for the formation of AgNPs was calculated from the changes of intensity of absorbance of aggregates of derivative **3** in the presence of Ag^+ ions at different time interval[2].

From the time vs. absorbance plot at fixed wavelength 470 nm by using first order rate equation we get the rate constant = k = slope×2.303 = 8.31×10^{-5} sec^{-1}.

---

[1] Luty-Błocho, M.; Pacławski, K.; Wojnicki, M.; Fitzner, K. *Inorganica Chimica Acta* **2013**, 395 189‑196.

[2] (a) Sau, T. K.; Murphy, C. J. *Langmuir* **2004**, *20*, 6414. (b) Goswami, S.; Das, S.; Aich, K.; Sarkar, D.; Mondal, T. K.; Quah, C. K.; Fun, H-K. *Dalton Trans*. **2013**, *42*, 15113–15119.

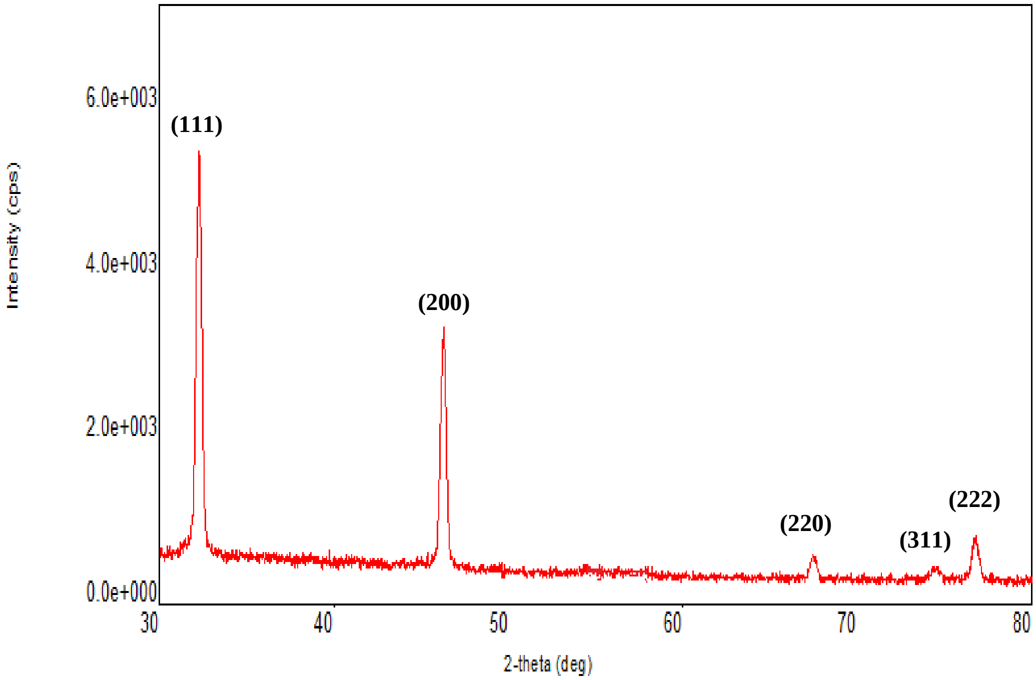

Fig. S4 Representative XRD diffraction patterns of AgNPs generated by derivative **3**.

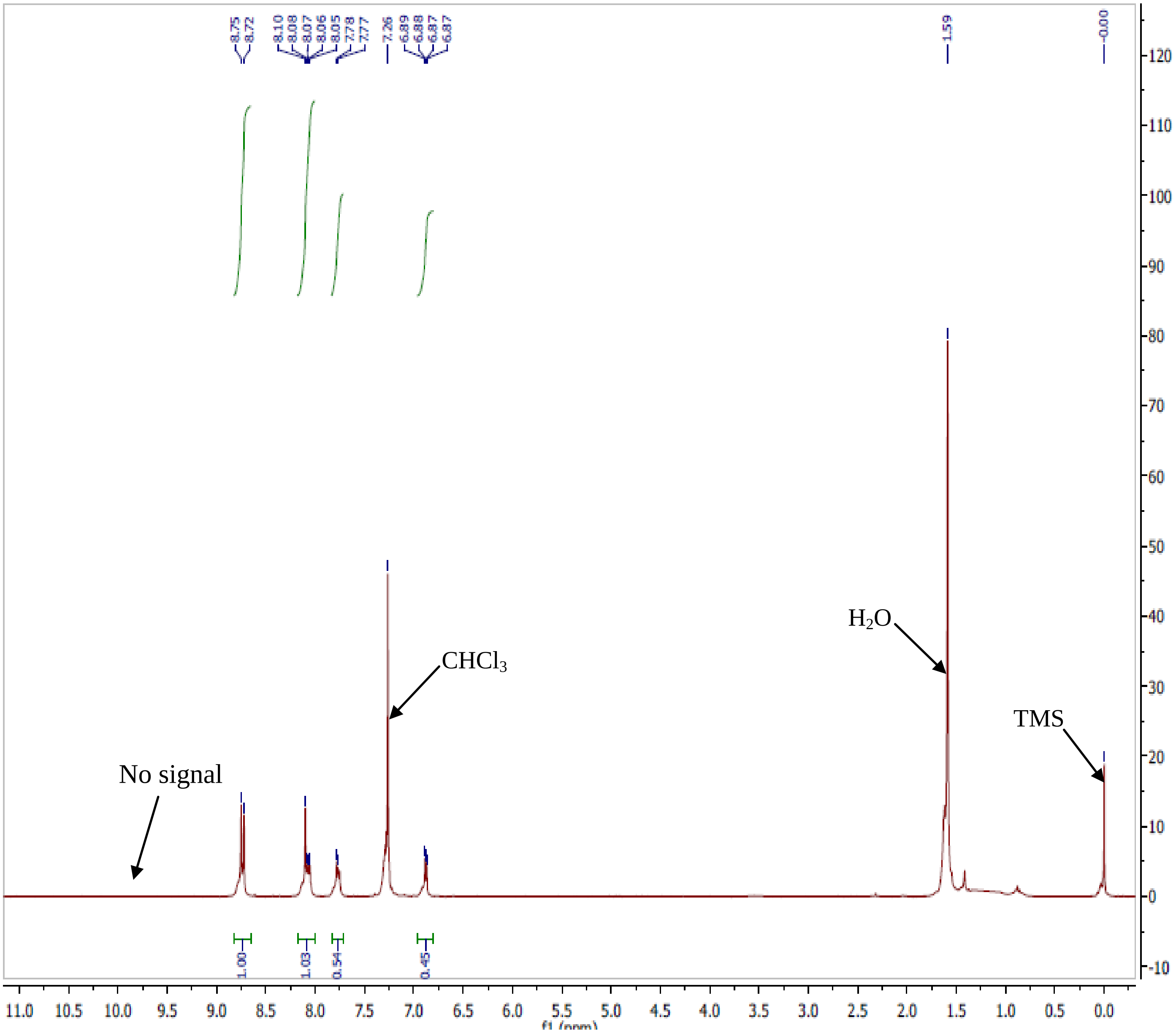

Fig. S5 ^1H NMR spectrum of residue obtained after washing precipitates with THF in $CDCl_3$.

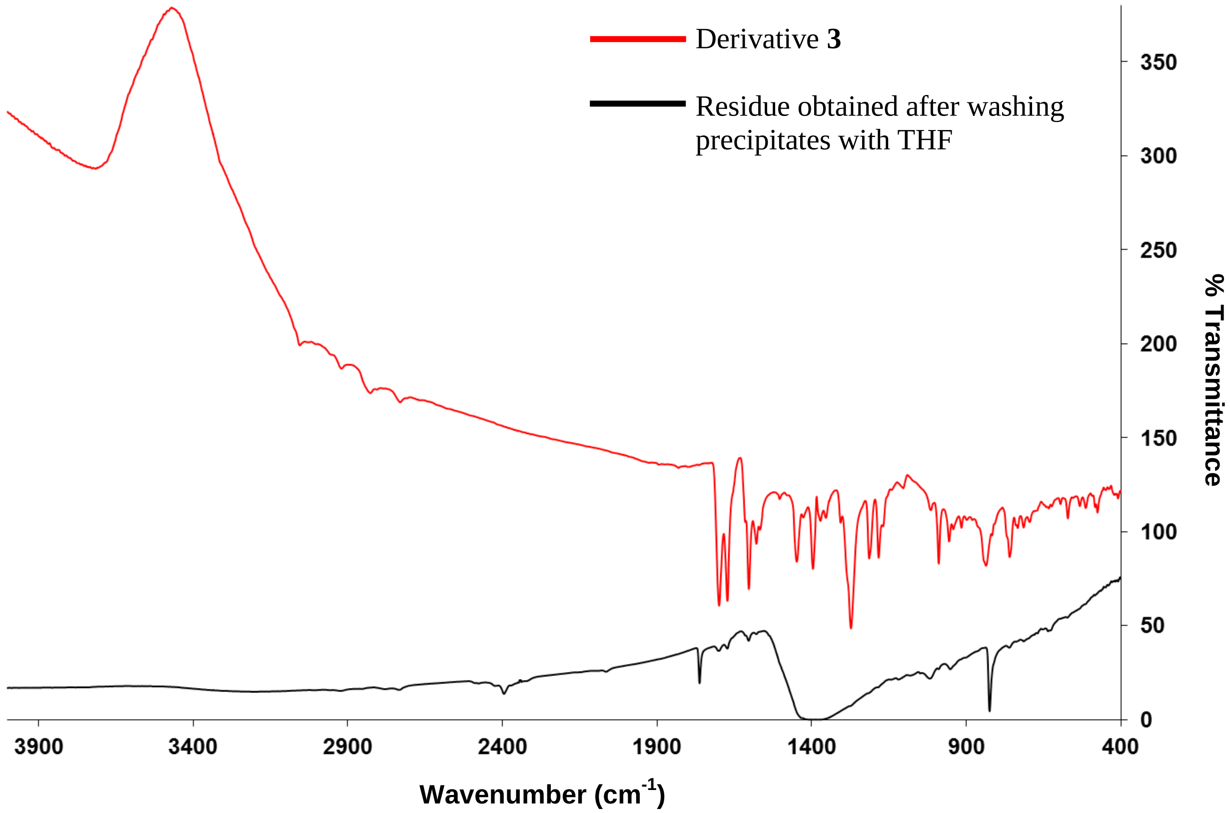

Fig. S6 Fourier transforms infrared absorption spectra of derivative **3** and the residue obtained after washing precipitates with THF

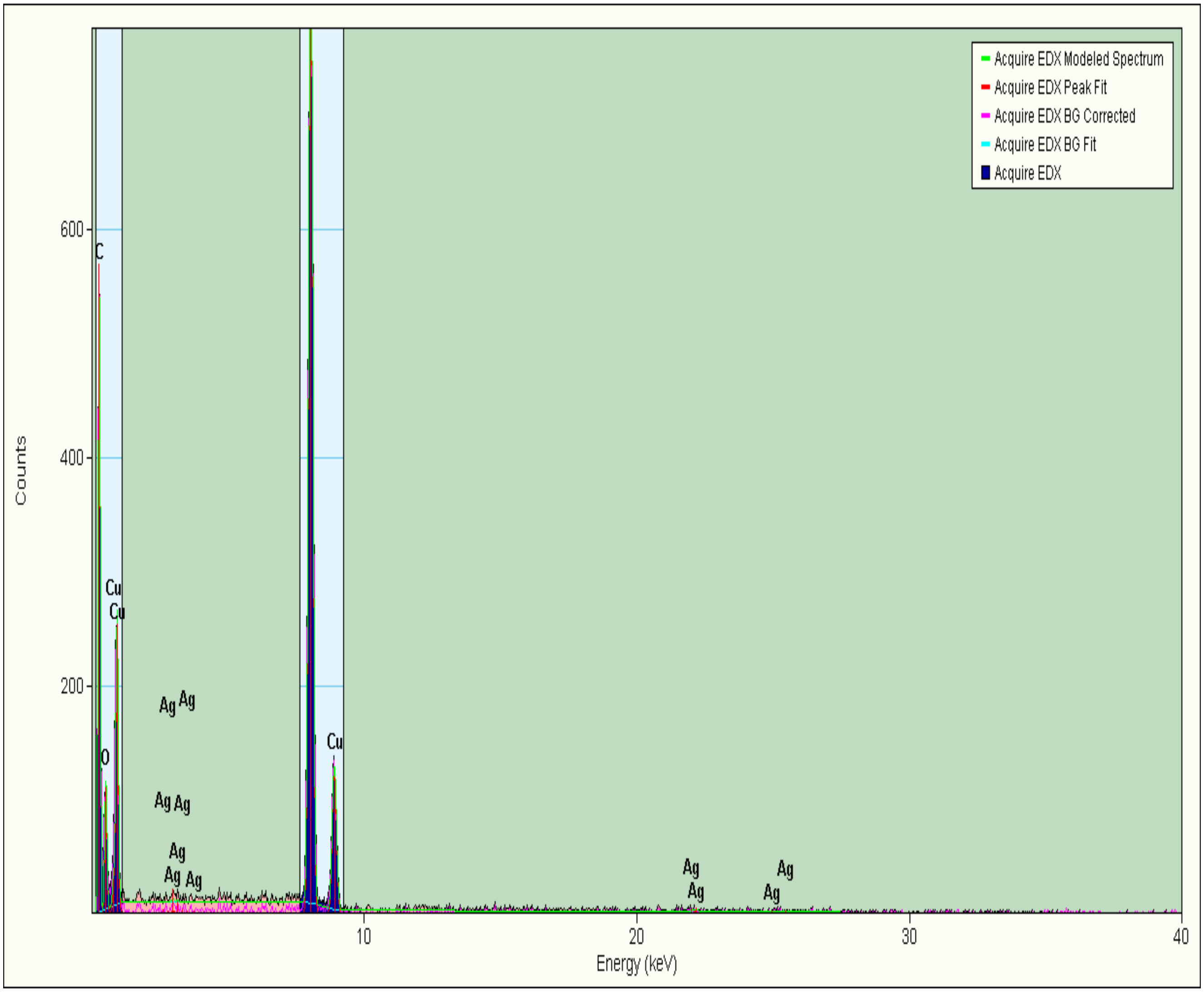

Fig. S7 Energy dispersive X-ray (EDX) analysis of the resulting precipitates supported on a copper grid.

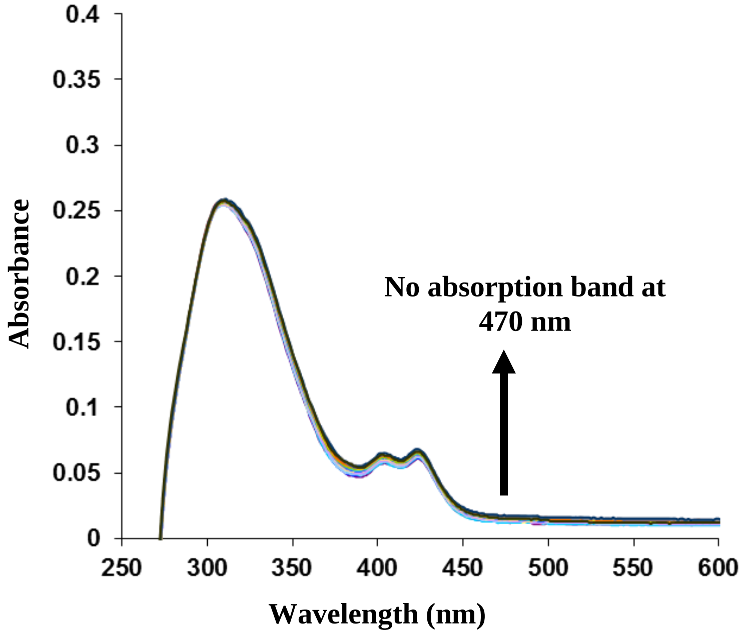

Fig. S8 UV-vis spectra of derivative **3** (10 μM) upon various additions of Ag^+ ions (100 equivalents) in pure THF.

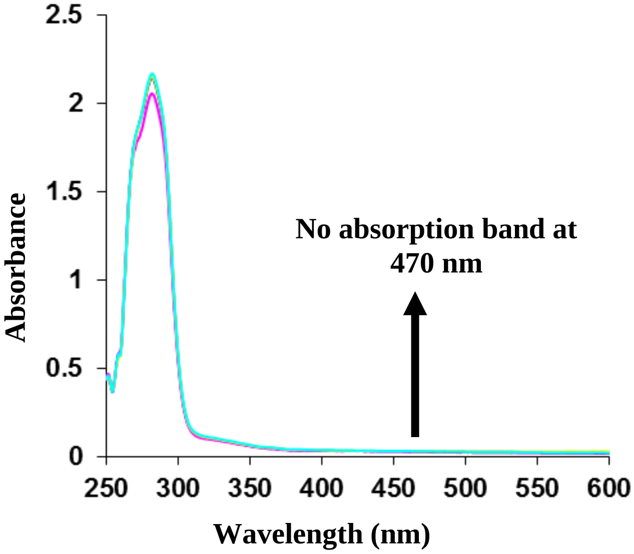

Fig. S9 UV-vis spectra of benzaldehyde (10 μM) upon various additions of Ag^+ ions (100 equivalents) in H_2O/THF (9.5/0.5).

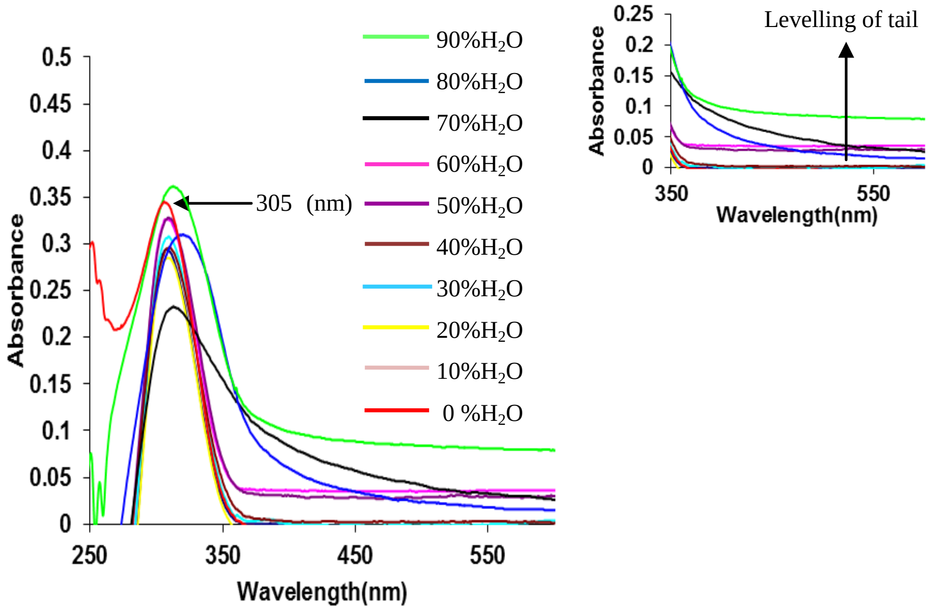

Fig. S10 UV-vis spectra showing the variation of absorbance of derivative **5** (10 μM) in H_2O/THF mixture with different fractions of H_2O. Inset: enlarge UV-vis spectra of derivative **5** (10 μM) with the addition of H_2O/THF mixture in the range of 350-600 nm showing level-off tail.

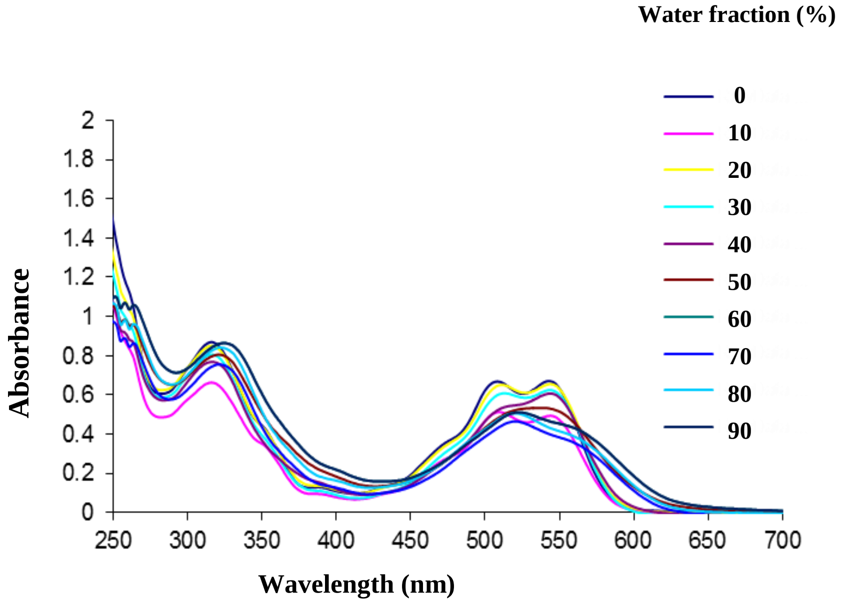

Fig. S11 UV-vis spectra showing the variation of absorbance of derivative **7** (10 μM) in H_2O/THF mixture with different fractions of H_2O.

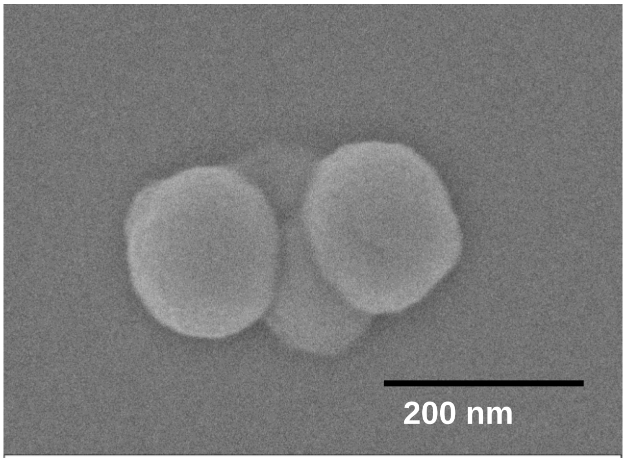

Fig. S12 SEM image of aggregates of derivative **5** in H_2O/THF (7/3) mixture. Scale bar 200 nm.

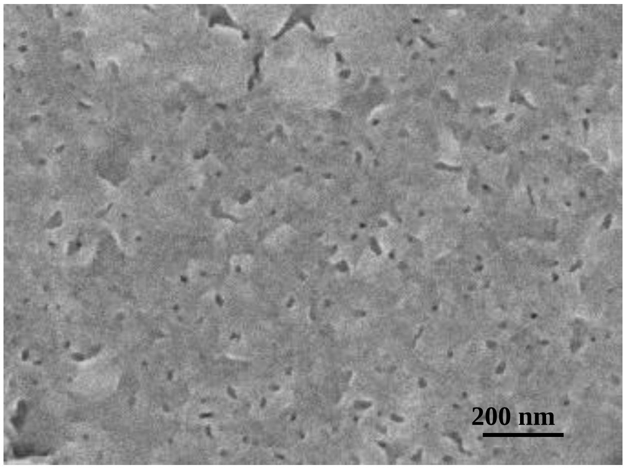

Fig. S13 SEM image of aggregates of derivative **7** in H_2O/THF (5/5) mixture. Scale bar 300 nm.

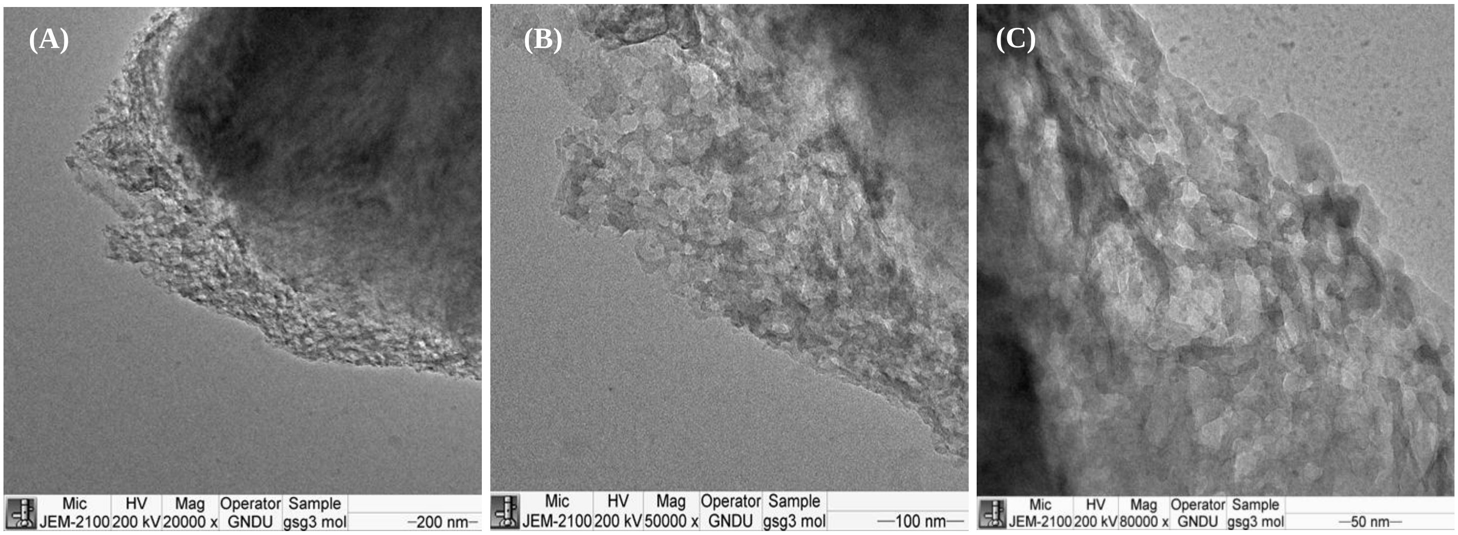

Fig. S14 TEM images of aggregates of derivative **7** in H_2O/THF (5/5) mixture showing porous morphology. Scale bar 50 nm.

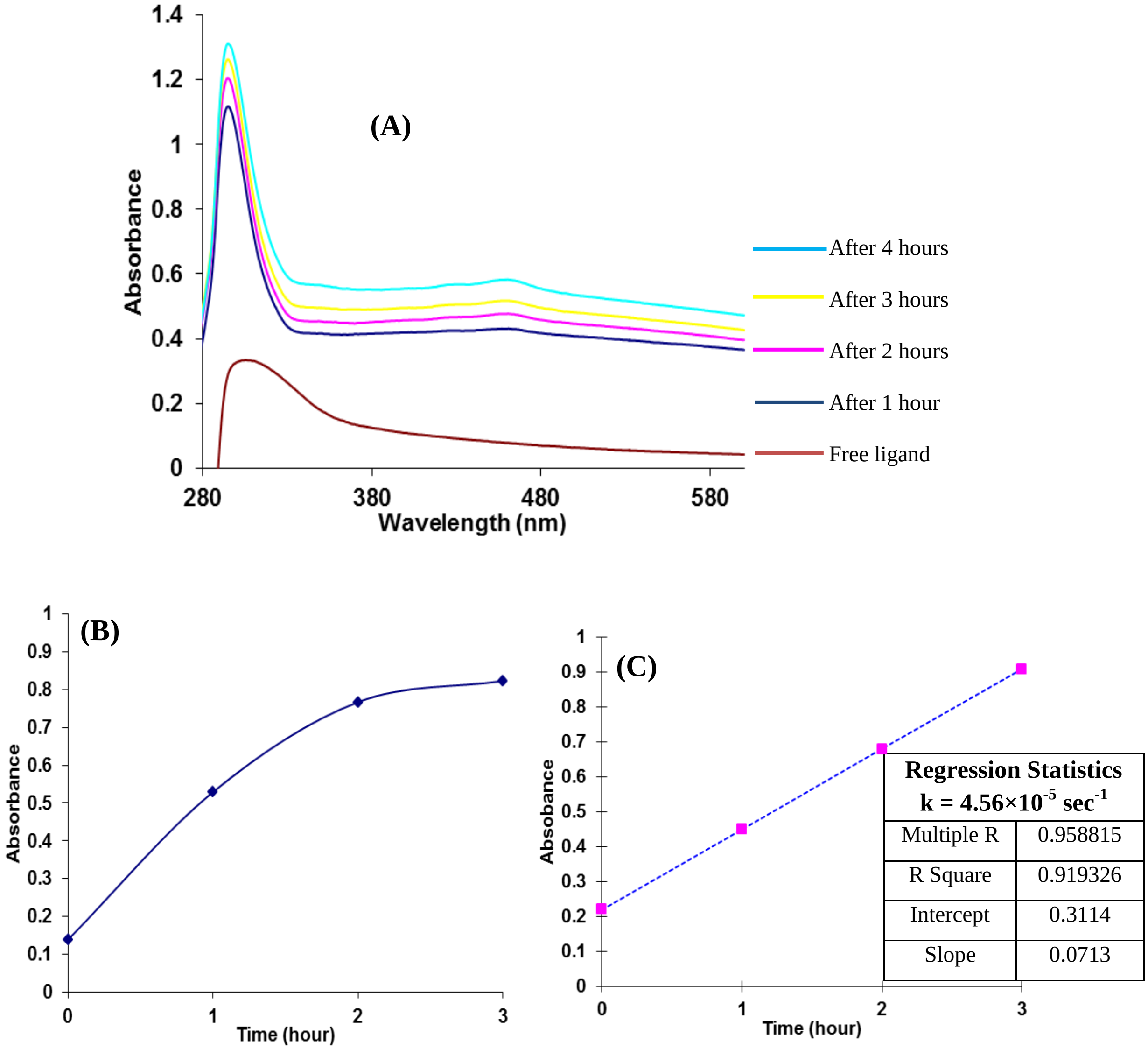

Fig. S15 (A) UV–visible spectra of derivative **5** (10 μm) upon addition of Ag$^+$ ions (200 equiv.) at different time intervals in H$_2$O/THF (7/3). Graphical representation of the rate of formation of AgNPs of derivative **5**. (B) Time (hours.) vs. absorbance plot at 460 nm (C) regression plot of B.

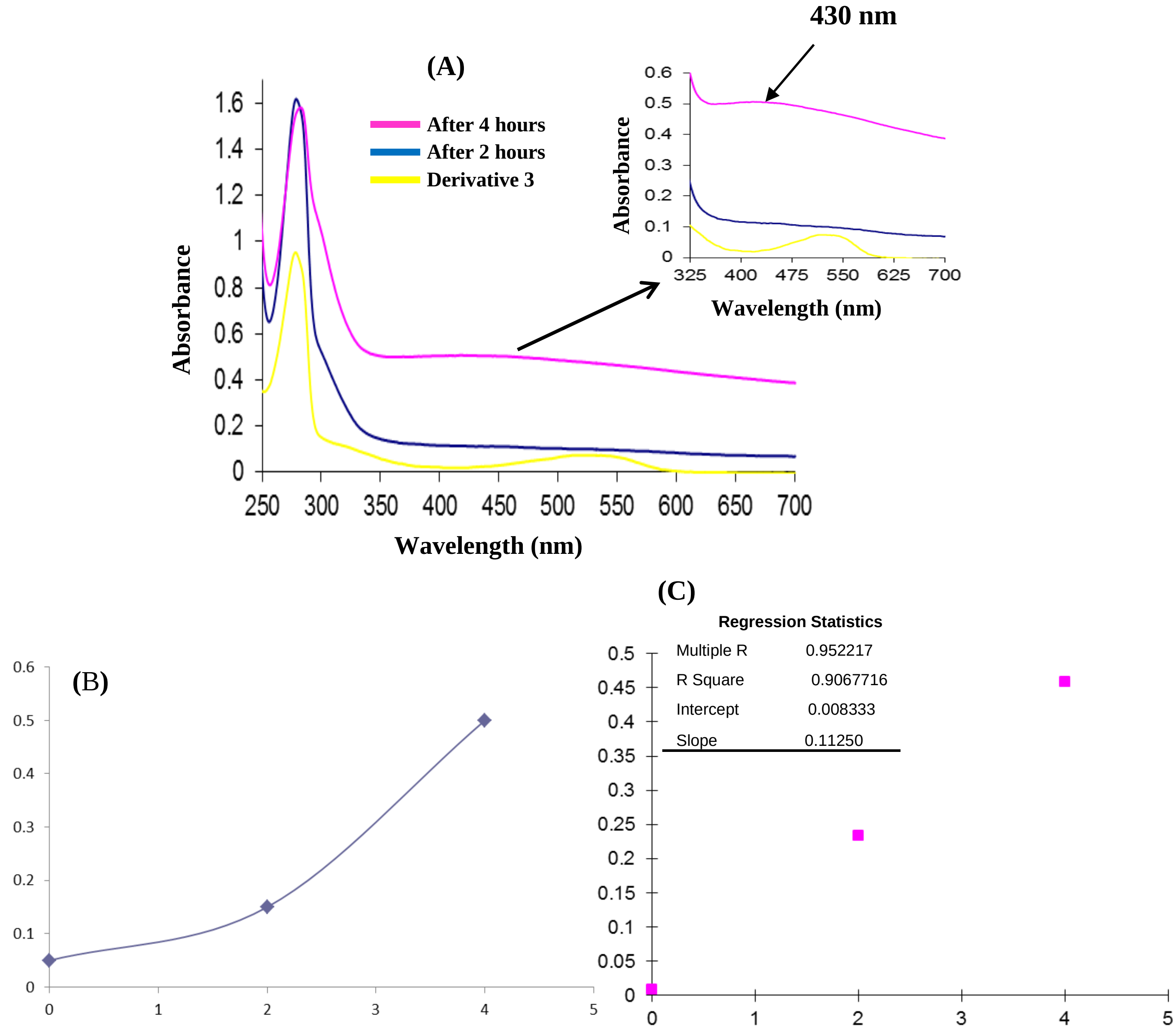

Fig. S16 (A) UV–visible spectra of derivative **7** (10 μm) upon addition of Ag^+ ions (200 equiv.) at different time intervals in H_2O/THF (5/5). Inset: enlarge UV-vis spectra of derivative **7** (10 μM) upon addition of Ag^+ ions in H_2O/THF (5/5) mixture in the range of 325-700 nm showing. band at 430 nm. Graphical representation of the rate of formation of AgNPs of derivative **7**. (B) Time (hours.) vs. absorbance plot at 430 nm (C) regression plot of B.

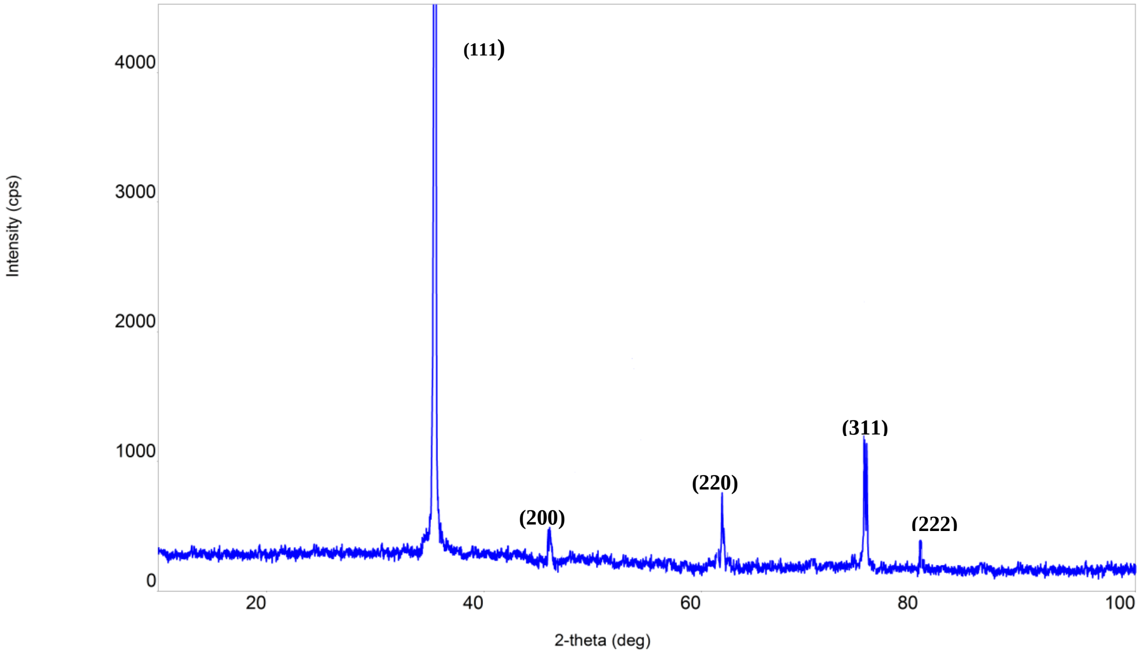

Fig. S17. Representative XRD diffraction pattern of AgNPs of derivative **5.**

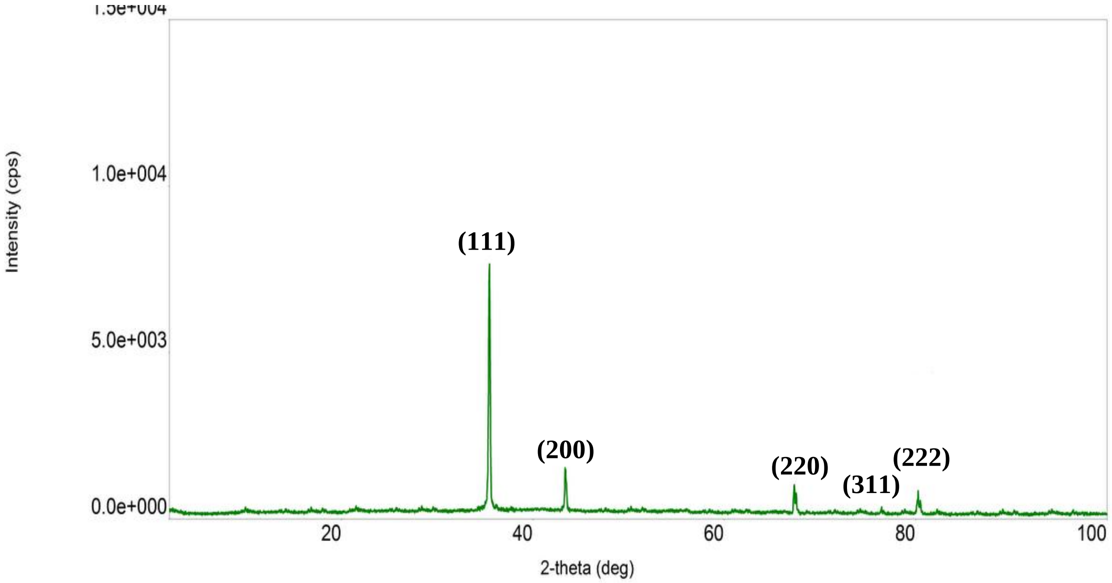

Fig. S18. Representative XRD diffraction pattern of AgNPs of derivative **7**

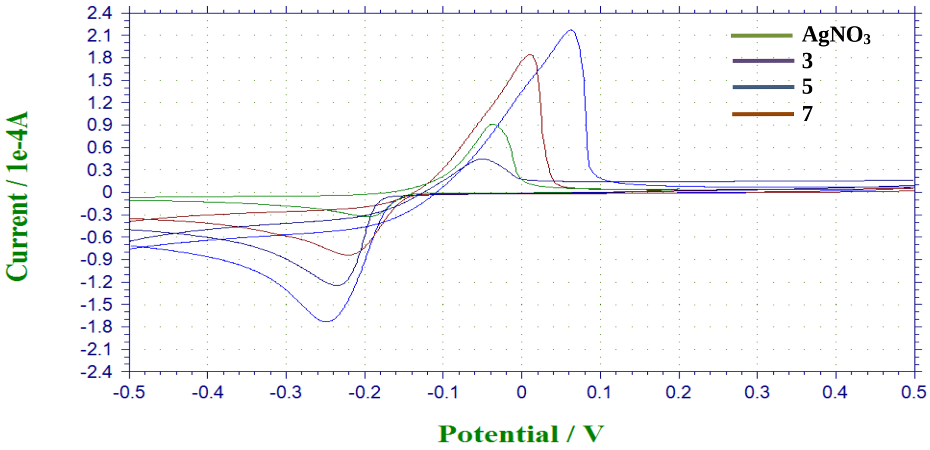

Fig. S19 Cyclic voltammograms of $AgNO_3$ and derivatives **3**, **5** and **7** in the presence of $AgNO_3$ in H_2O/ACN (1/9, v/v) mixture.

Table S3. Onsets of Cathodic Peaks (Volts) and Cathodic Peak Potentials (Volts) of $AgNO_3$ alone and $AgNO_3$ in the Presence of derivatives **3**, **5** and **7** (10 µM).

Sample	**Onset of cathodic peak**	**E_{pc}**
$AgNO_3$	-0.13 V	-0.19 V
3 + $AgNO_3$	-0.18 V	-0.235 V
5 + $AgNO_3$	-0.16 V	-0.249 V
7+ $AgNO_3$	-0.15 V	-0.220 V

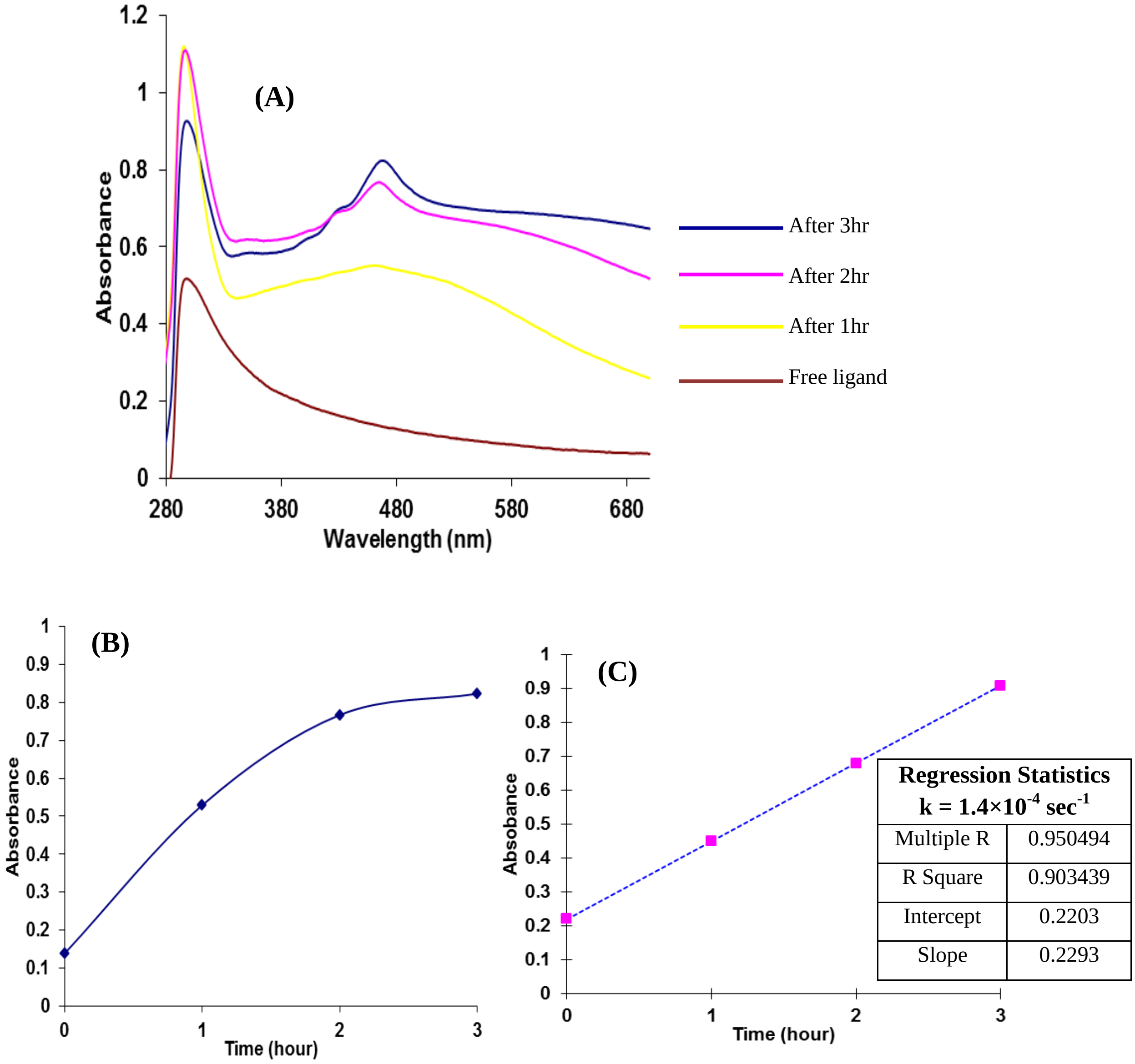

Regression Statistics **k = 1.4×10^{-4} sec^{-1}**	
Multiple R	0.950494
R Square	0.903439
Intercept	0.2203
Slope	0.2293

Fig. 20 UV–visible spectra of derivative **5** (10 μm) upon addition of Ag$^+$ ions (200 equiv.) at different time intervals in H_2O/THF (7/3) in the presence of KI (50 μL, 10 μM). Graphical representation of the rate of formation of AgNPs of derivative **5** in the presence of KI. showing rate constant (B) Time (hours.) vs. absorbance plot at 460 nm (C) regression plot of B.

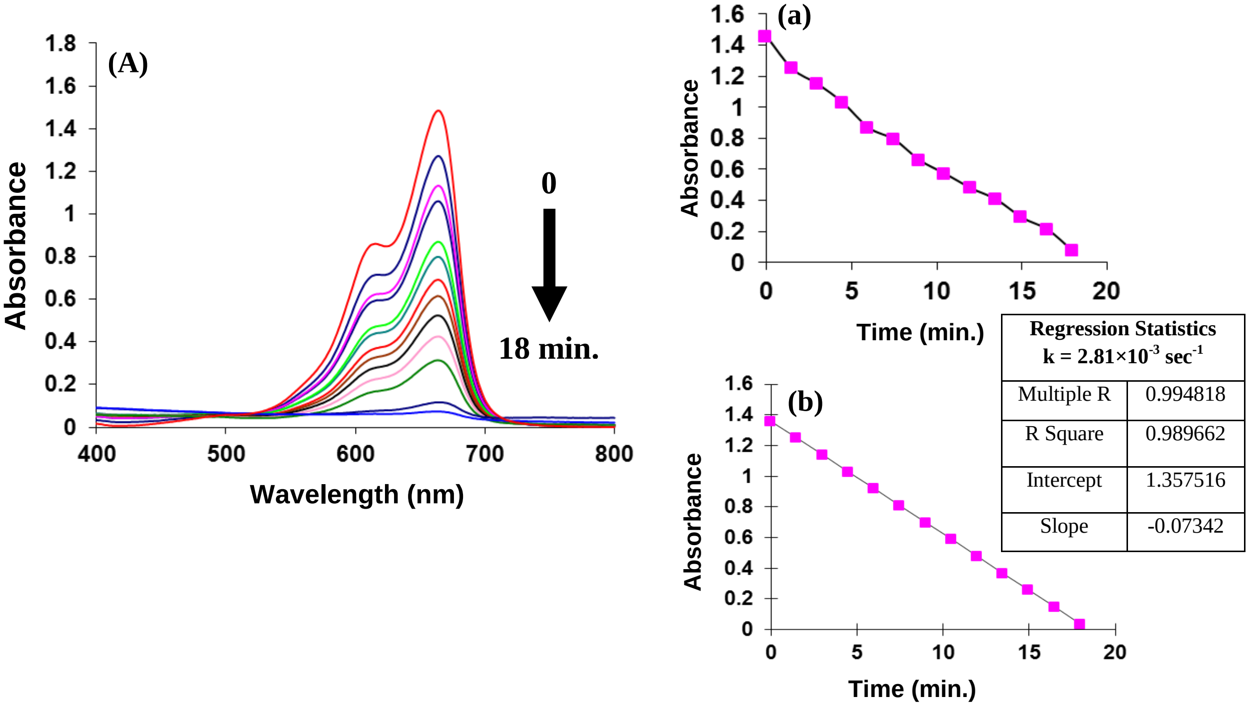

Regression Statistics **k = 2.81×10^{-3} sec^{-1}**	
Multiple R	0.994818
R Square	0.989662
Intercept	1.357516
Slope	-0.07342

Fig. S21 (A) Decrease in methylene blue absorbance at 665 nm over time using *in-situ* generated AgNPs by derivative **3** as catalyst in the presence of $NaBH_4$ (B) Normalized kinetic trace of the absorbance at 665 nm during the degradation of methylene blue. (C) Kinetic rate constant.

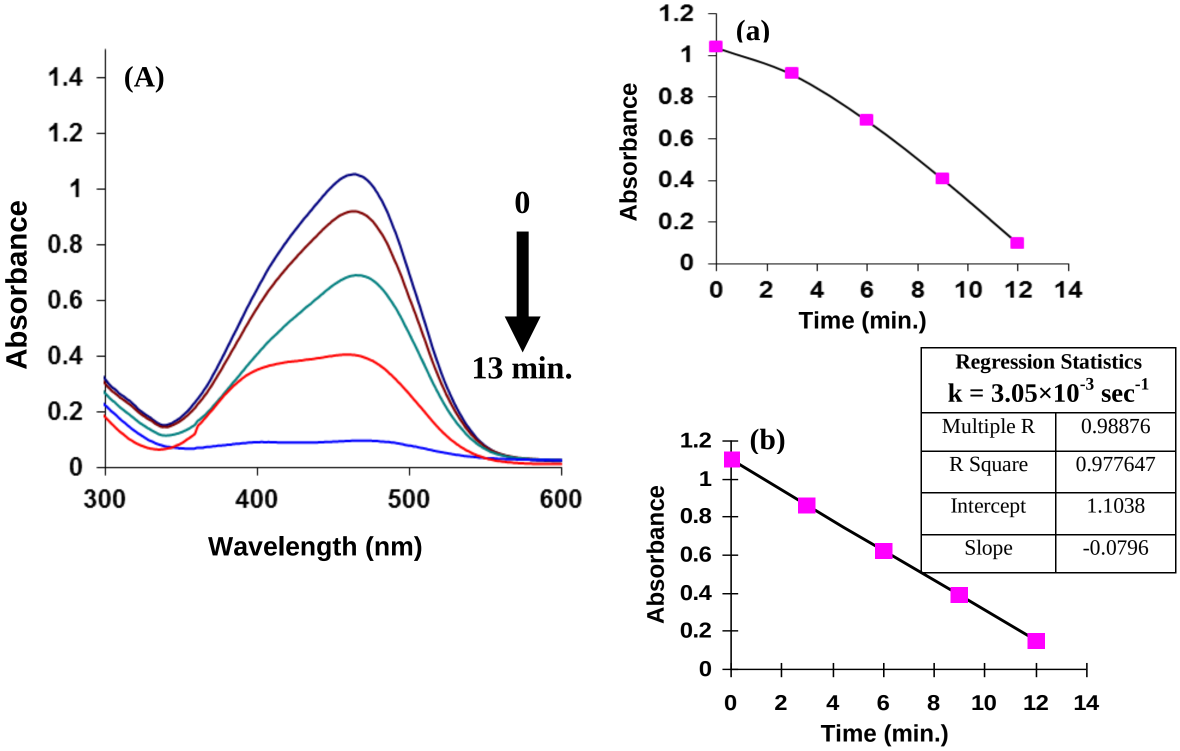

Regression Statistics **k = 3.05×10^{-3} sec^{-1}**	
Multiple R	0.98876
R Square	0.977647
Intercept	1.1038
Slope	-0.0796

Fig. S22 (A) Decrease in methyl orange absorbance at 465 nm over time using *in-situ* generated AgNPs by derivative **3** as catalyst in the presence of $NaBH_4$ (B) Normalized kinetic trace of the absorbance at 465 nm during the degradation of methyl orange. (C) Kinetic rate constant.

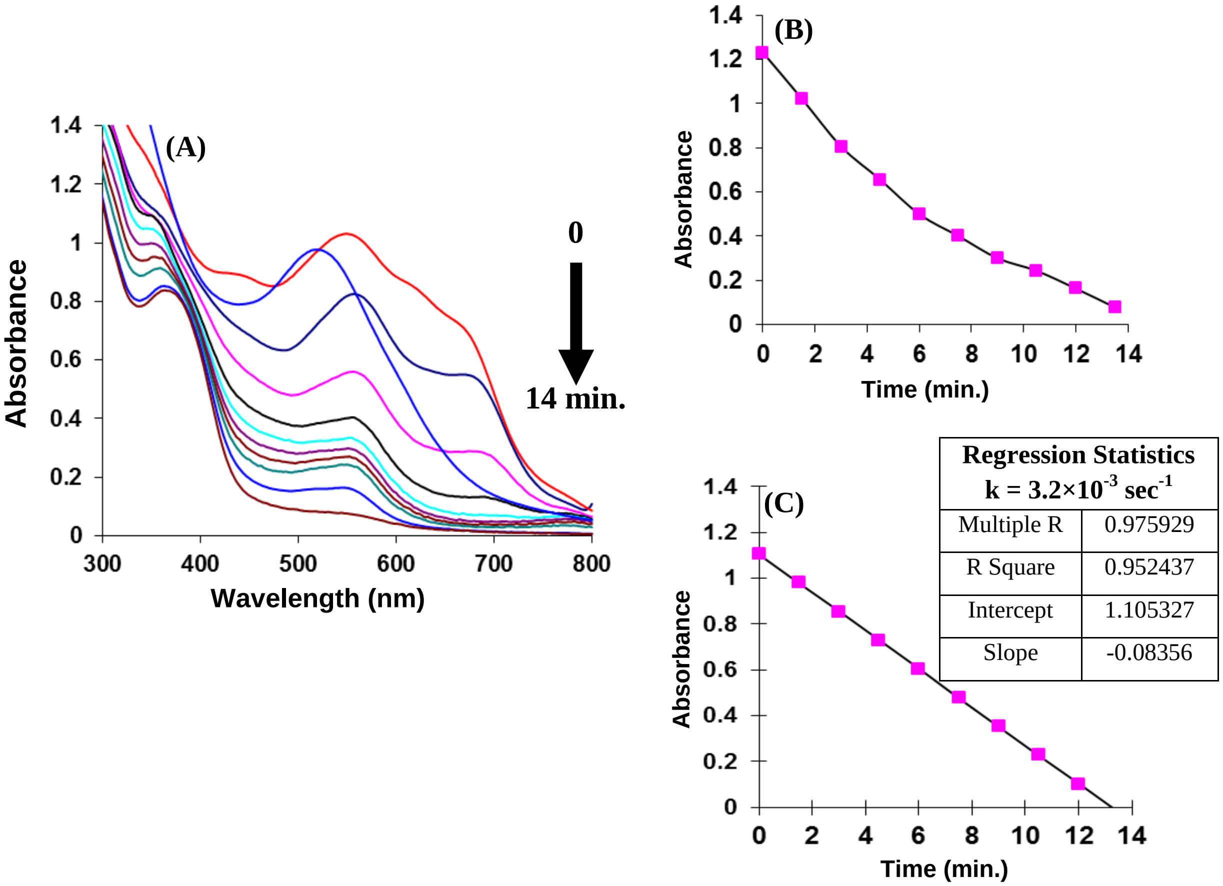

Regression Statistics k = 3.2×10^{-3} sec^{-1}	
Multiple R	0.975929
R Square	0.952437
Intercept	1.105327
Slope	-0.08356

Fig. S23 (A) Decrease in eriochrome black T absorbance at 545 nm over time using *in-situ* generated AgNPs by derivative **3** as catalyst in the presence of NaBH$_4$ (B) Normalized kinetic trace of the absorbance at 545 nm during the degradation of eriochrome black T. (C) Kinetic rate constant.

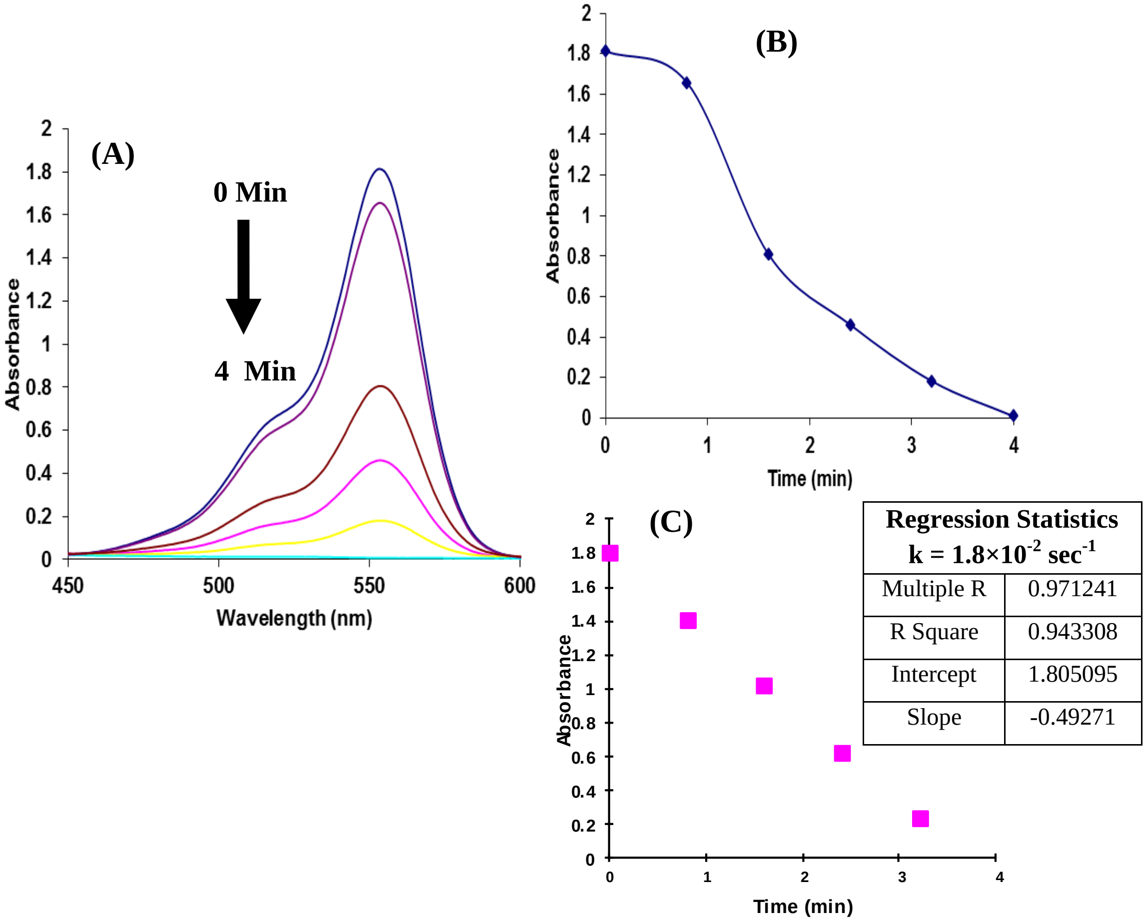

Regression Statistics **k = 1.8×10^{-2} sec^{-1}**	
Multiple R	0.971241
R Square	0.943308
Intercept	1.805095
Slope	-0.49271

Fig. S24 (A) Decrease in rhodamine B absorbance at 554 nm over time using *in-situ* generated AgNPs by derivative **5** as catalyst in the presence of NaBH$_4$ (B) Normalized kinetic trace of the absorbance at 554 nm during the degradation of rhodamine B. (C) Kinetic rate constant.

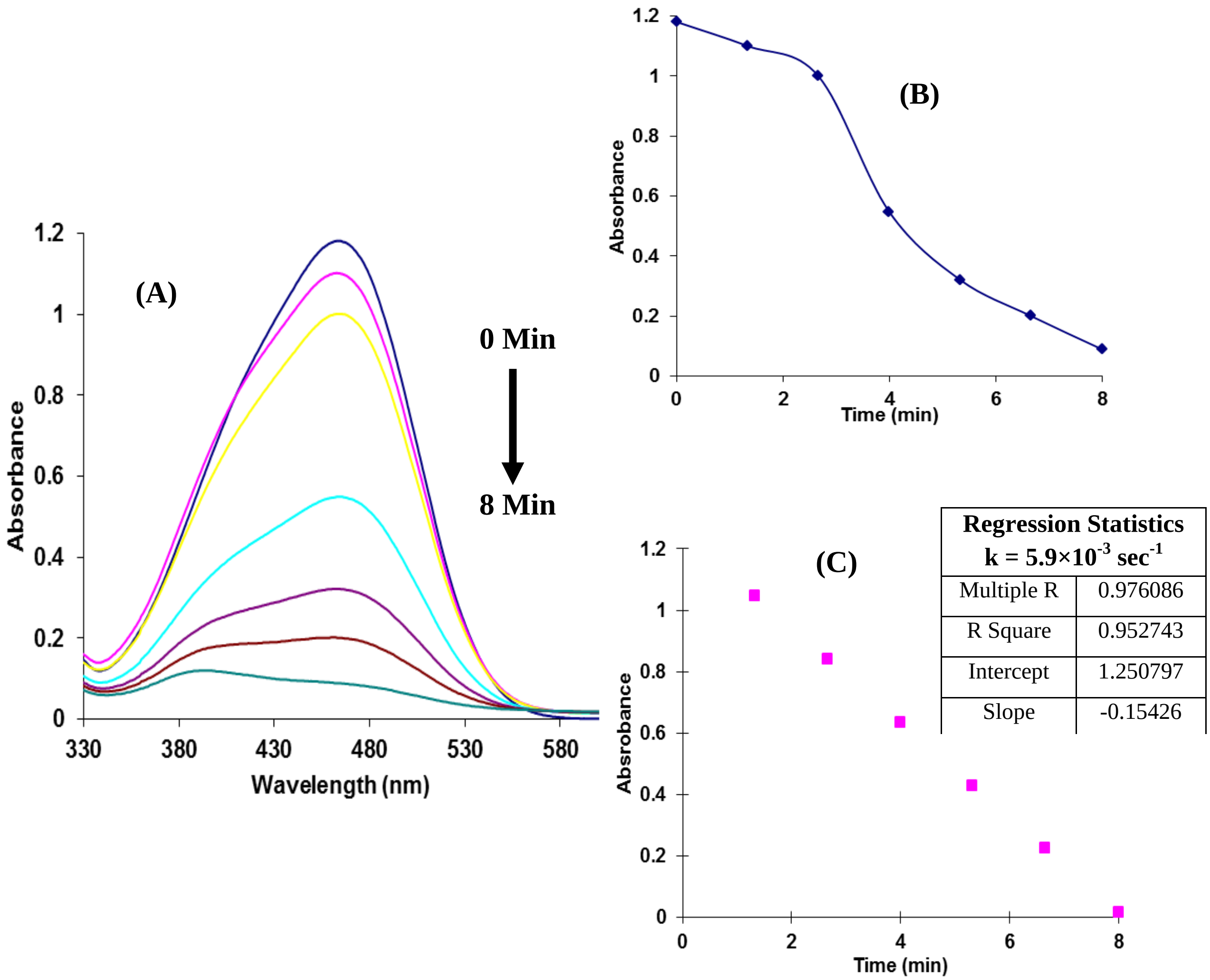

Regression Statistics **k = 5.9×10^{-3} sec^{-1}**	
Multiple R	0.976086
R Square	0.952743
Intercept	1.250797
Slope	-0.15426

Fig. S25 (A) Decrease in methyl orange absorbance at 465 nm over time using *in-situ* generated AgNPs by derivative **5** as catalyst in the presence of NaBH$_4$ (B) Normalized kinetic trace of the absorbance at 465 nm during the degradation of methyl orange. (C) Kinetic rate constant.

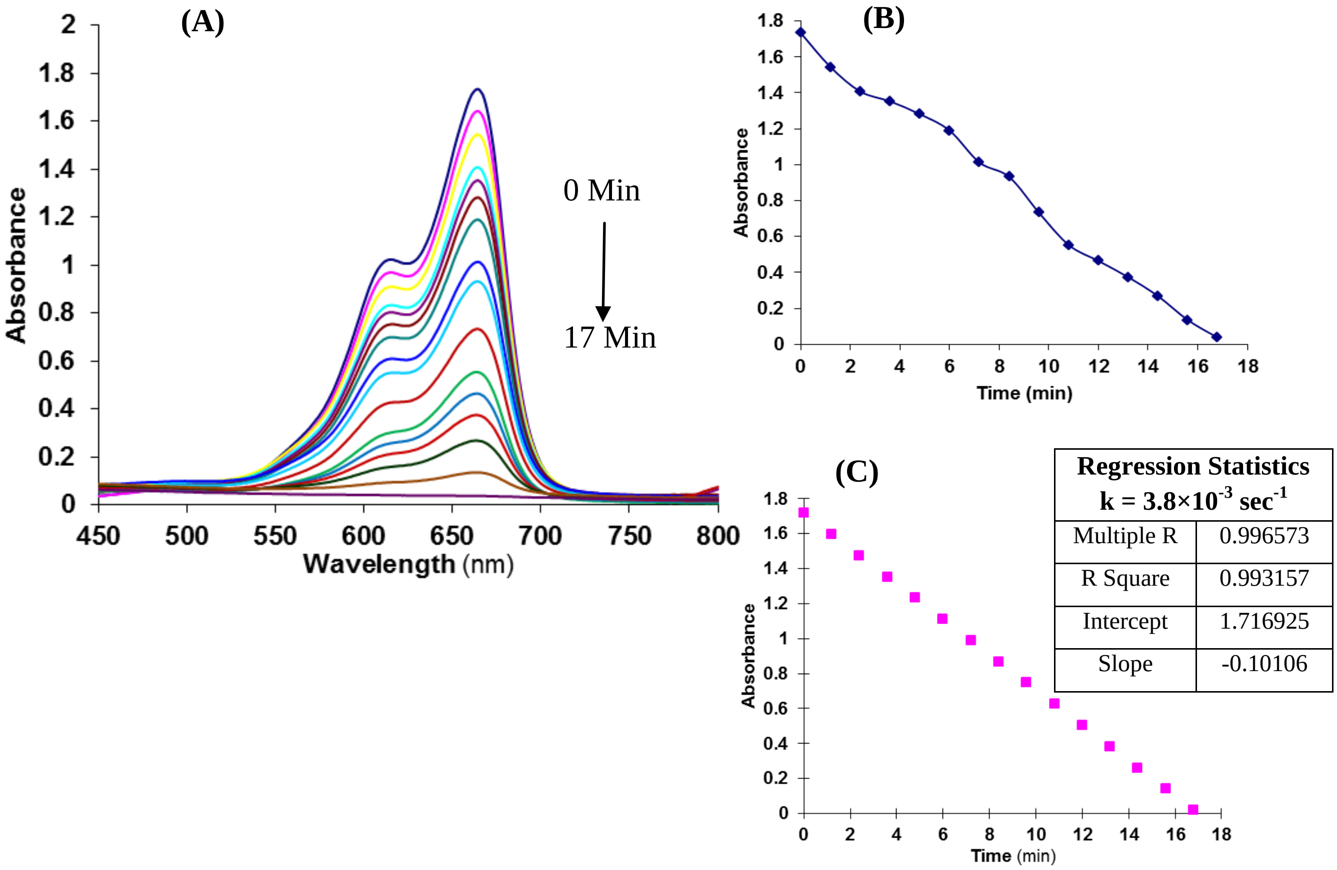

Regression Statistics **k = 3.8×10^{-3} sec^{-1}**	
Multiple R	0.996573
R Square	0.993157
Intercept	1.716925
Slope	-0.10106

Fig. S26 (A) Decrease in methylene blue absorbance at 665 nm over time using *in-situ* generated AgNPs by derivative **5** as catalyst in the presence of $NaBH_4$ (B) Normalized kinetic trace of the absorbance at 665 nm during the degradation of methylene blue. (C) Kinetic rate constant.

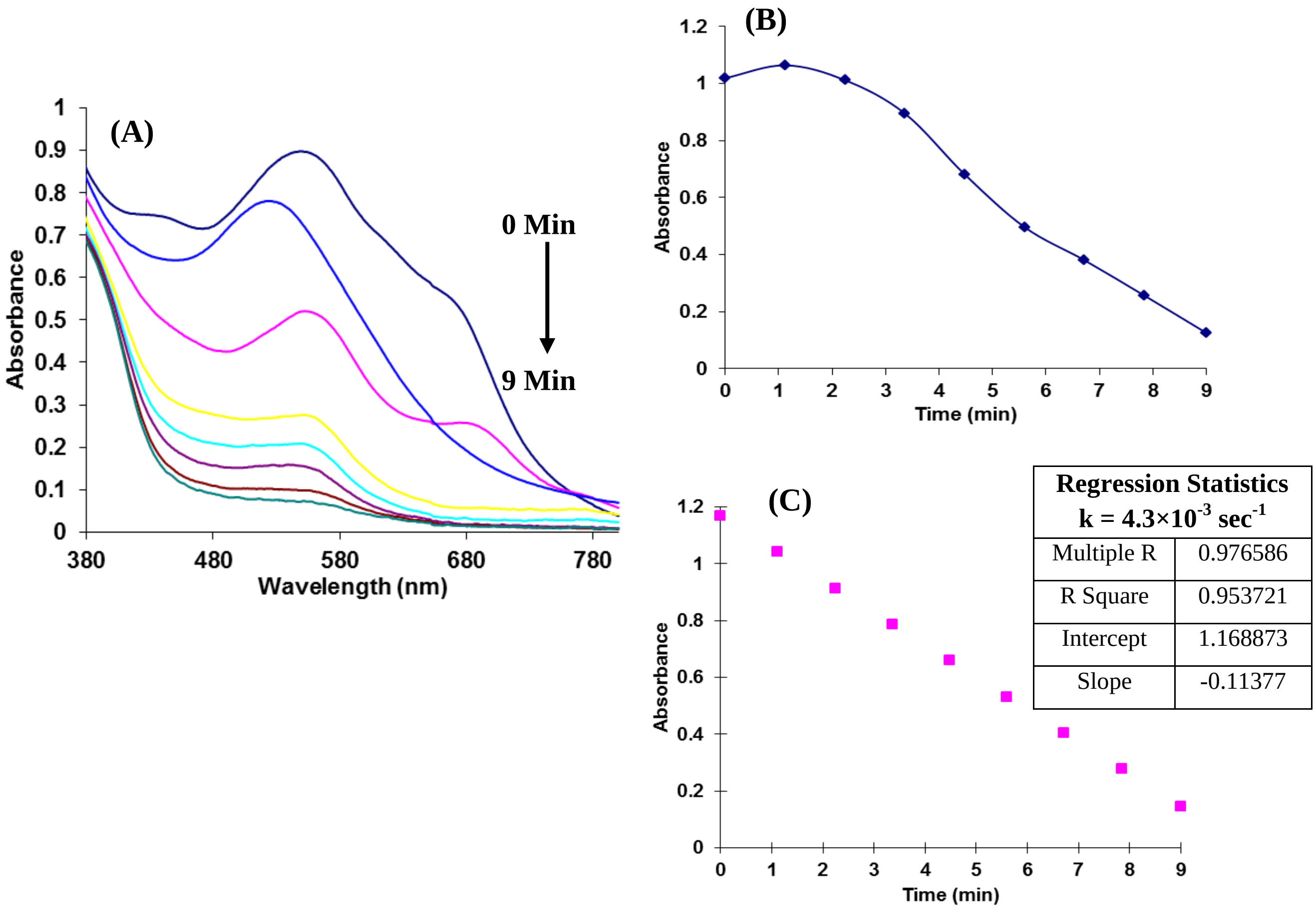

Regression Statistics k = 4.3×10^{-3} sec^{-1}	
Multiple R	0.976586
R Square	0.953721
Intercept	1.168873
Slope	-0.11377

Fig. S27 (A) Decrease in eriochrome black T absorbance at 545 nm over time using *in-situ* generated AgNPs by derivative **5** as catalyst in the presence of NaBH$_4$ (B) Normalized kinetic trace of the absorbance at 554 nm during the degradation of eriochrome black T. (C) Kinetic rate constant.

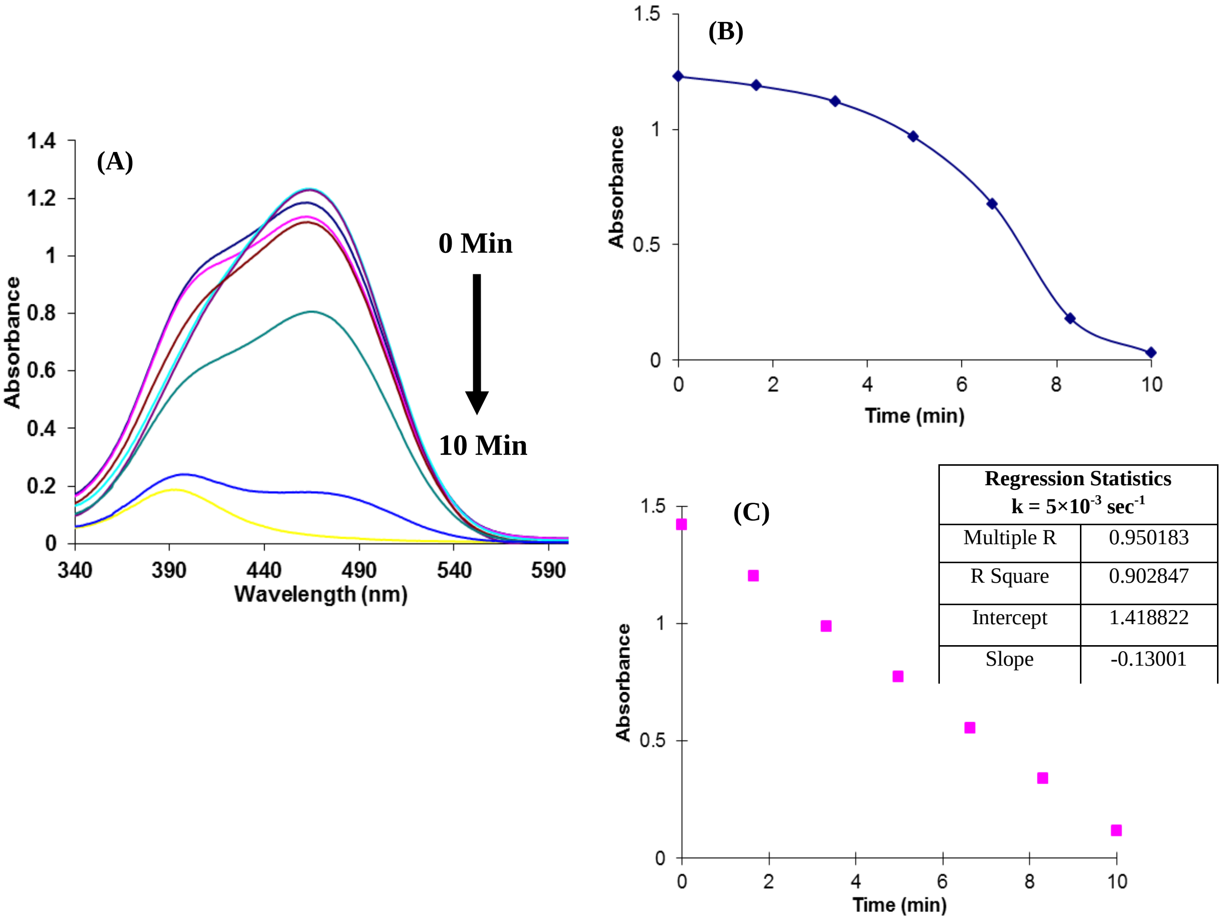

Regression Statistics k = 5×10^{-3} sec^{-1}	
Multiple R	0.950183
R Square	0.902847
Intercept	1.418822
Slope	-0.13001

Fig. S28 (A) Decrease in methyl orange absorbance at 465 nm over time using *in-situ* generated AgNPs by derivative **7** as catalyst in the presence of $NaBH_4$ (B) Normalized kinetic trace of the absorbance at 465 nm during the degradation of methyl orange. (C) Kinetic rate constant.

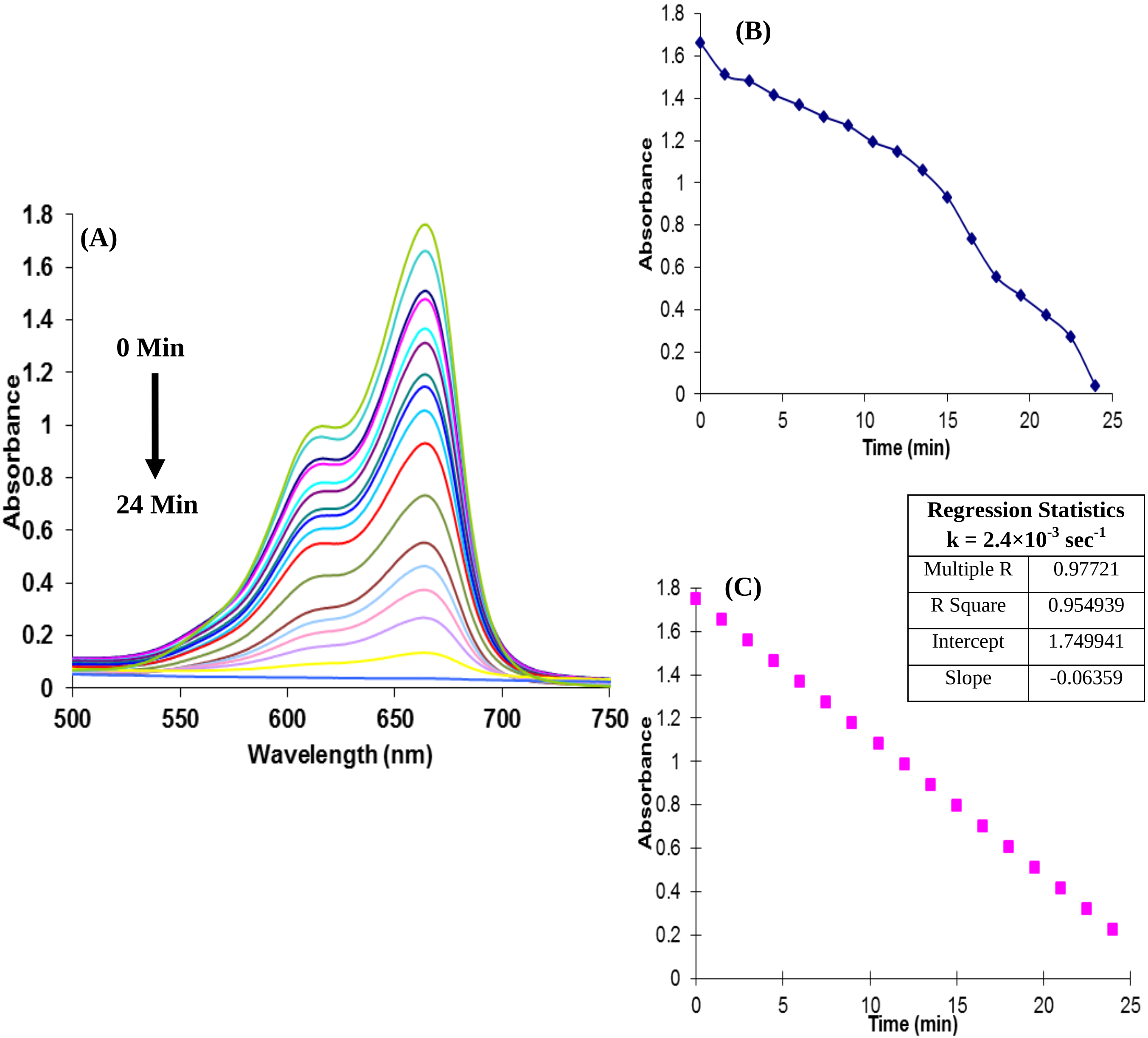

Regression Statistics **k = 2.4×10^{-3} sec^{-1}**	
Multiple R	0.97721
R Square	0.954939
Intercept	1.749941
Slope	-0.06359

Fig. S29 (A) Decrease in methylene blue absorbance at 665 nm over time using *in-situ* generated AgNPs by derivative **7** as catalyst in the presence of $NaBH_4$ (B) Normalized kinetic trace of the absorbance at 665 nm during the degradation of methylene blue. (C) Kinetic rate constant.

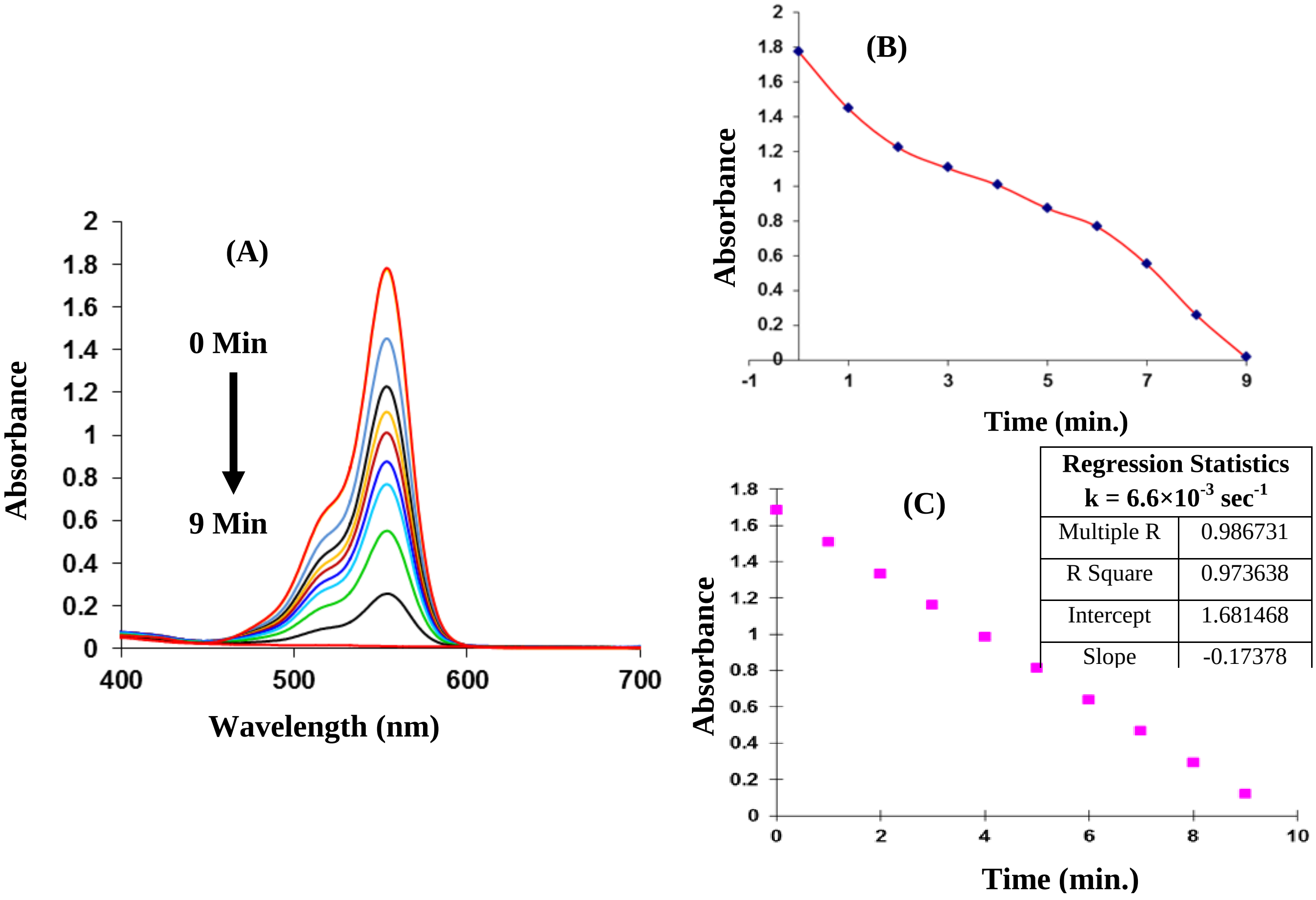

Regression Statistics **k = 6.6×10^{-3} sec^{-1}**	
Multiple R	0.986731
R Square	0.973638
Intercept	1.681468
Slope	-0.17378

Fig. S30 (A) Decrease in Rhodamine B absorbance at 554 nm over time using *in-situ* generated AgNPs by derivative **7** as catalyst in the presence of NaBH$_4$ (B) Normalized kinetic trace of the absorbance at 554 nm during the degradation of Rhodamine B. (C) Kinetic rate constant.

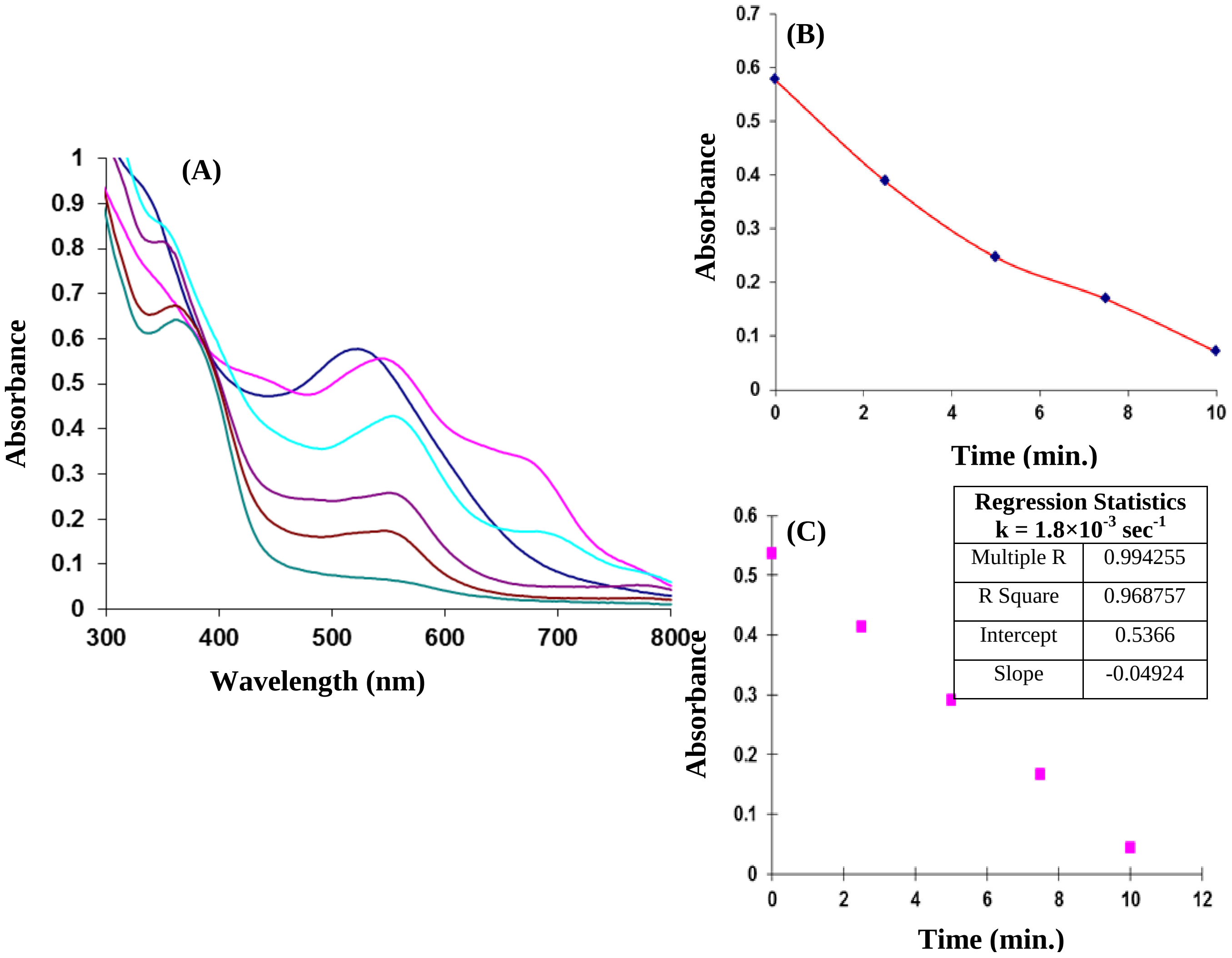

Regression Statistics k = 1.8×10^{-3} sec^{-1}	
Multiple R	0.994255
R Square	0.968757
Intercept	0.5366
Slope	-0.04924

Fig. S31 (A) Decrease in eriochrome black T absorbance at 545 nm over time using *in-situ* generated AgNPs by derivative **7** as catalyst in the presence of $NaBH_4$ (B) Normalized kinetic trace of the absorbance at 545 nm during the degradation of eriochrome black T. (C) Kinetic rate constant.

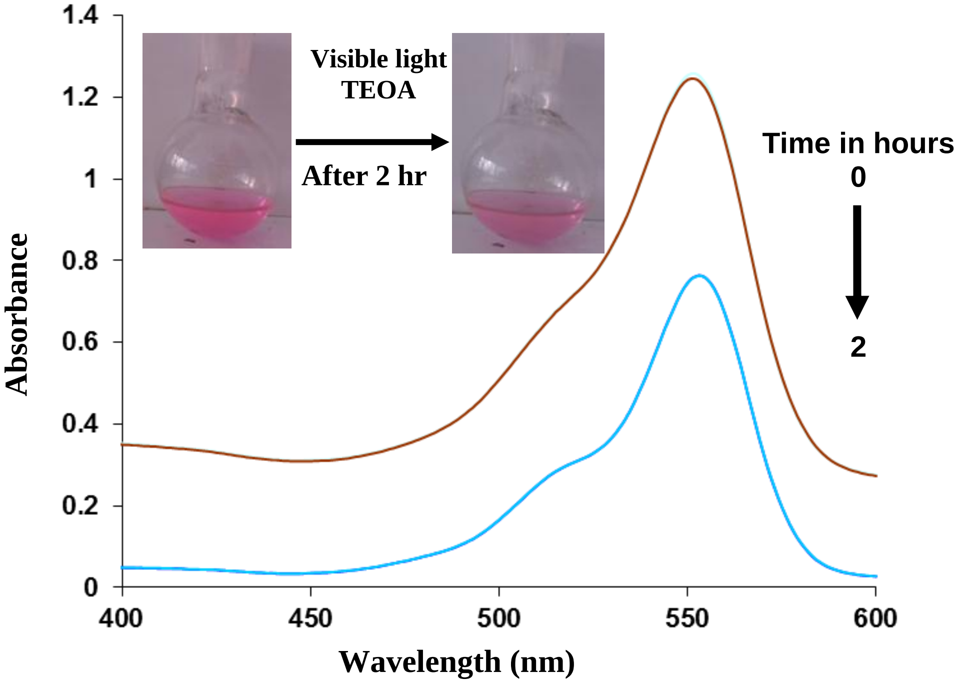

Fig. 32 UV-vis spectral changes of RhB over time using derivative **3**-stabilized AgNPs as catalyst under visible light irradiations in the presence of triethanolamine (TEOA). Inset: photographs show colour change of aqueous RhB solution after 2 hours under visible light irradiations in the presence of

Procedure for the catalyst-reusing sequence in the AgNPs-catalyzed degradation of RhB : The catalytic degradation of Rhodamine B in the presence of $NaBH_4$ aqueous solution was chosen as a model reaction to investigate the reusability of *in-situ* generated AgNPs catalyst by derivatives **3**, **5** and **7**. Firstly, same volume of aqueous solution of $NaBH_4$ (0.2 M) and RhB (2 mM) solution were mixed to obtain the mixture solution of $NaBH_4$ and RhB dye and diluted 100 times in deionized water. Addition of catalytic amount of *in-situ* generated AgNPs solution by derivative **3** (10 µL, 10 nmol), **5** (10 µL, 20 nmol) and **7** (10 µL, 20 nmol) to the solution of RhB results in colour change from pink to colourless. After the catalytic degradation of Rhodamine B, resulting reaction mixture containing AgNPs catalyst was subjected at least three times (in case of AgNPs of derivatives **3** and **5**) and five times (AgNPs of derivative **7**) to reaction for the next catalytic sequence by adding Rhodamine B (50 µL, 2 mM) and $NaBH_4$ (50 µL, 0.2 mM) to the reaction mixture.

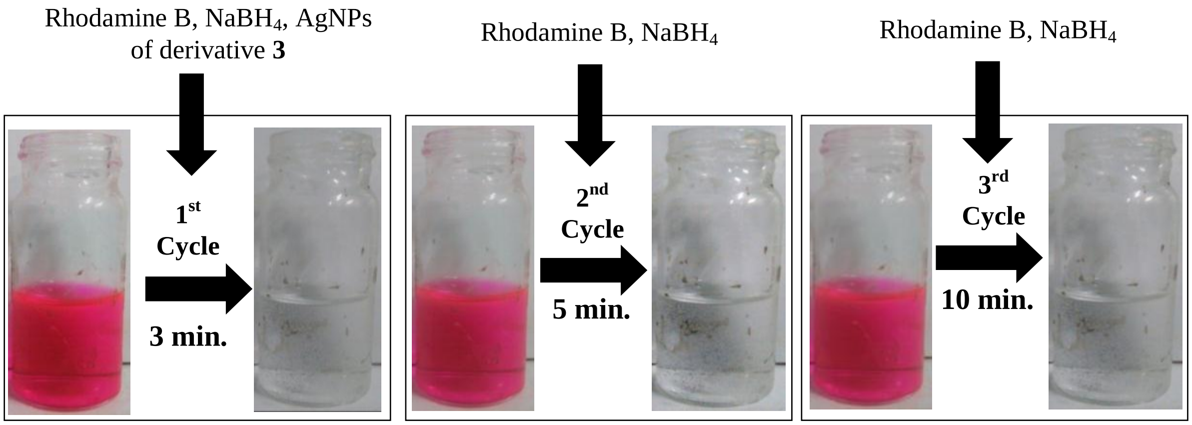

Fig. S33 Depiction of reusing of derivative **3** stabilized AgNPs catalyst.

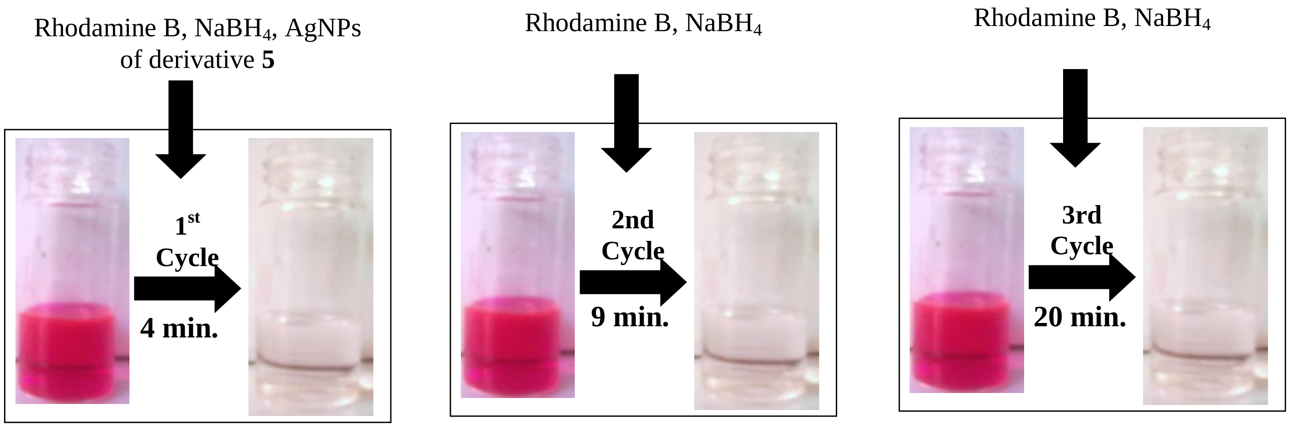

Fig. S34 Depiction of reusing of derivative **5** stabilized AgNPs catalyst.

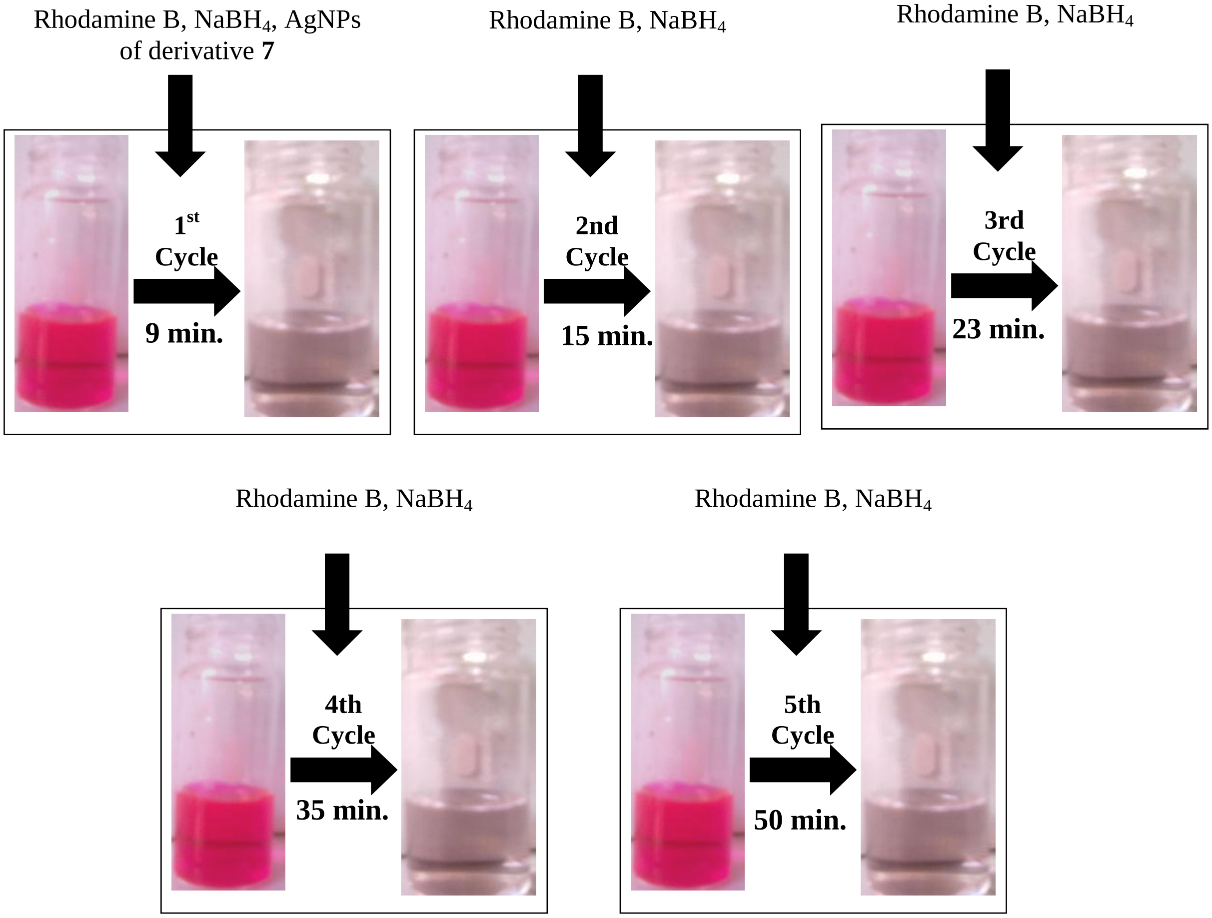

Fig. S35 Depiction of reusing of derivative **7** stabilized AgNPs catalyst.

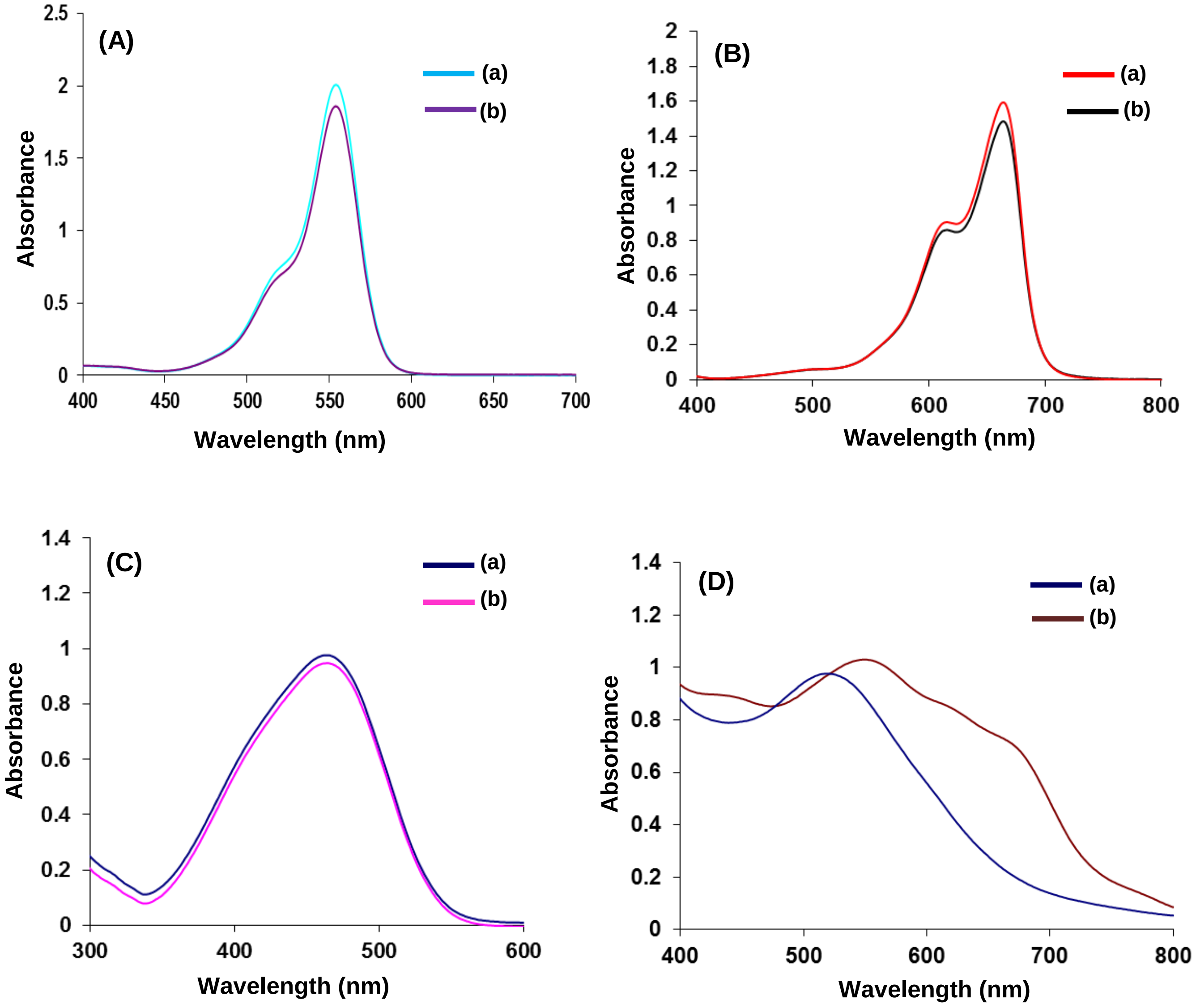

Fig. S36 UV-visible spectra for the degradation of (A) Rhodamine B (B) methylene blue (C) methyl orange and (D) eriochrome black T using $NaBH_4$ in the absence of AgNPs catalyst: (a) 0 min and (b) after 24 hours.

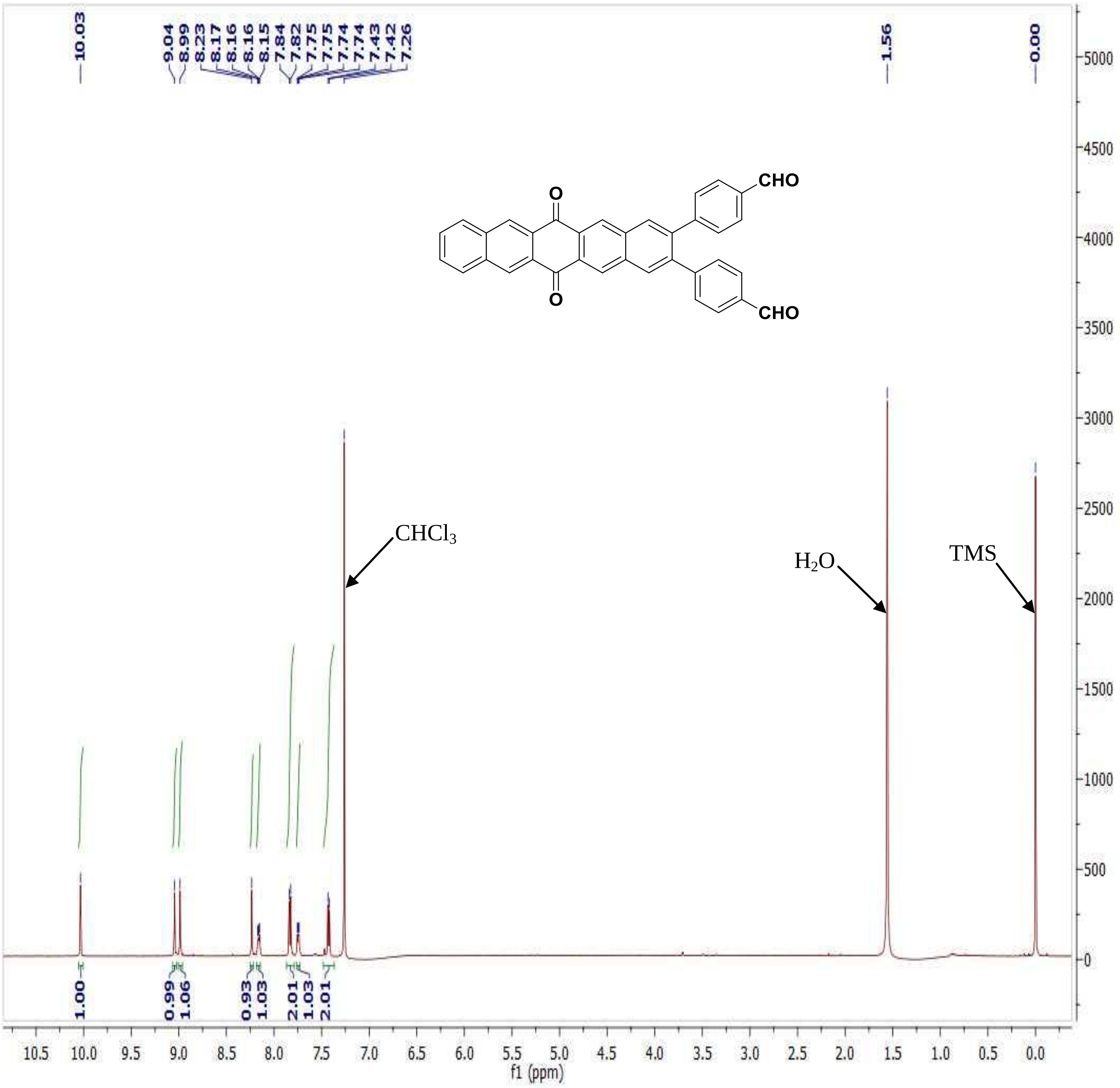

Fig. S37 ^{1}H NMR spectrum of derivative **3** in $CDCl_3$.

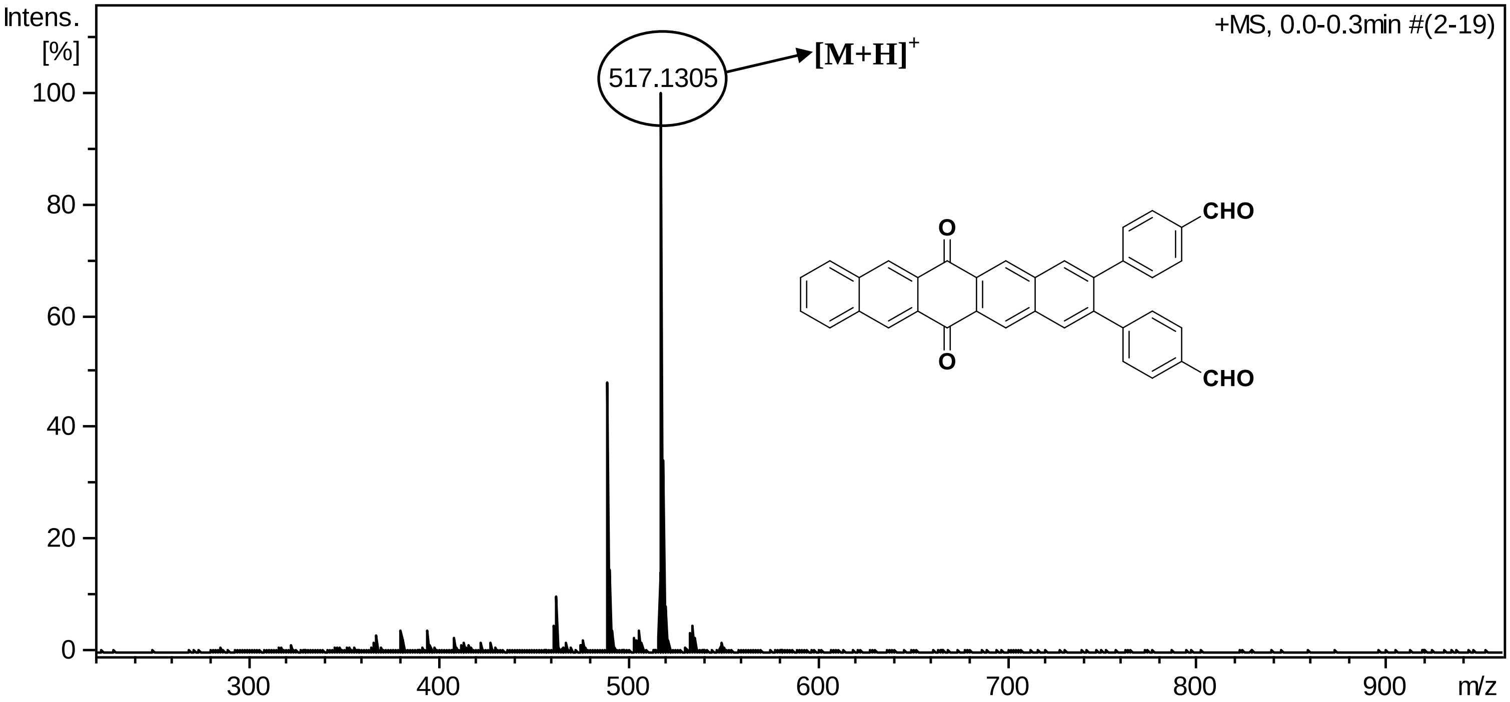

Fig. S38 Mass spectrum of derivative **3**.

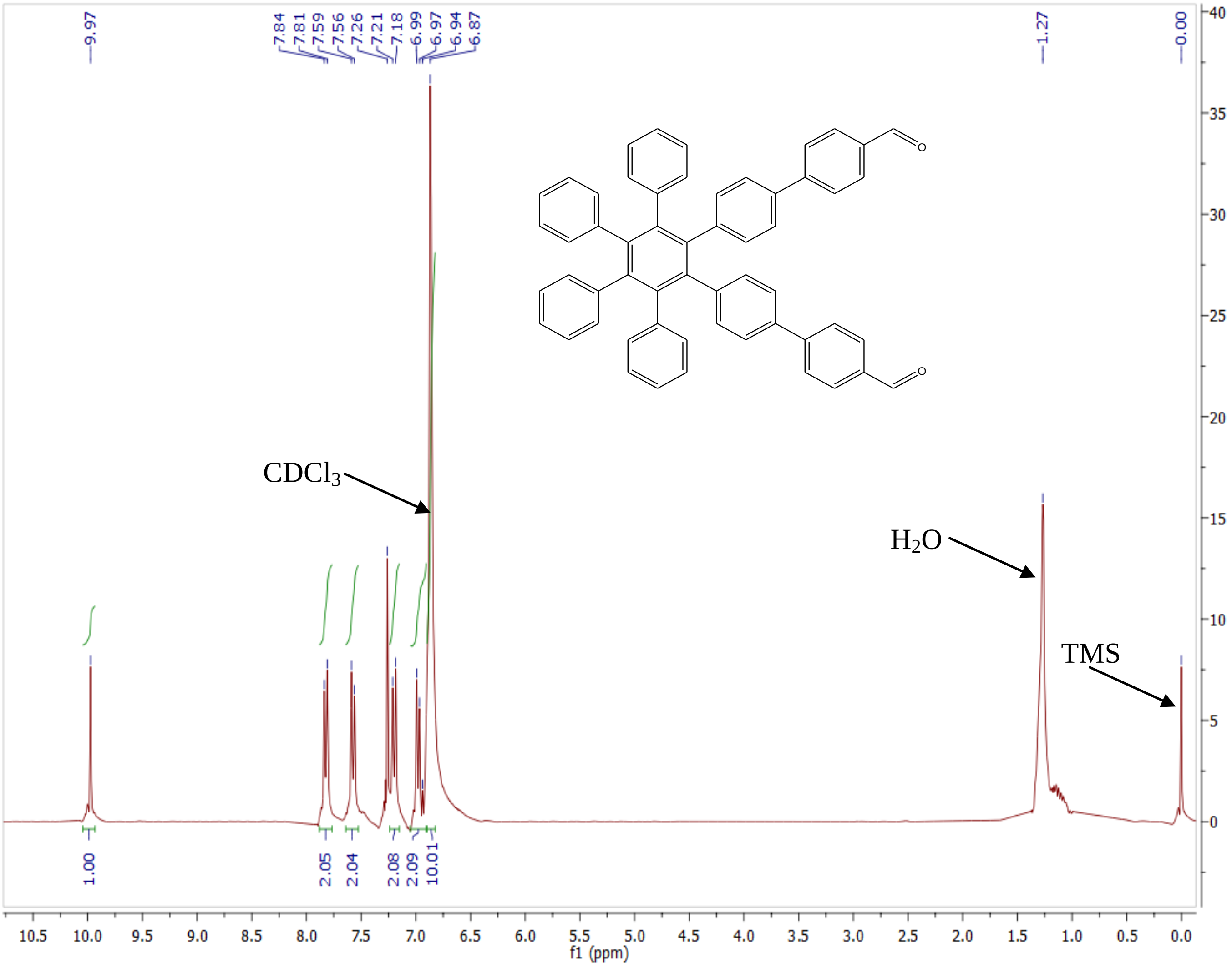

Fig. 39 ^{1}H NMR spectrum of derivative **5** in CDCl$_3$

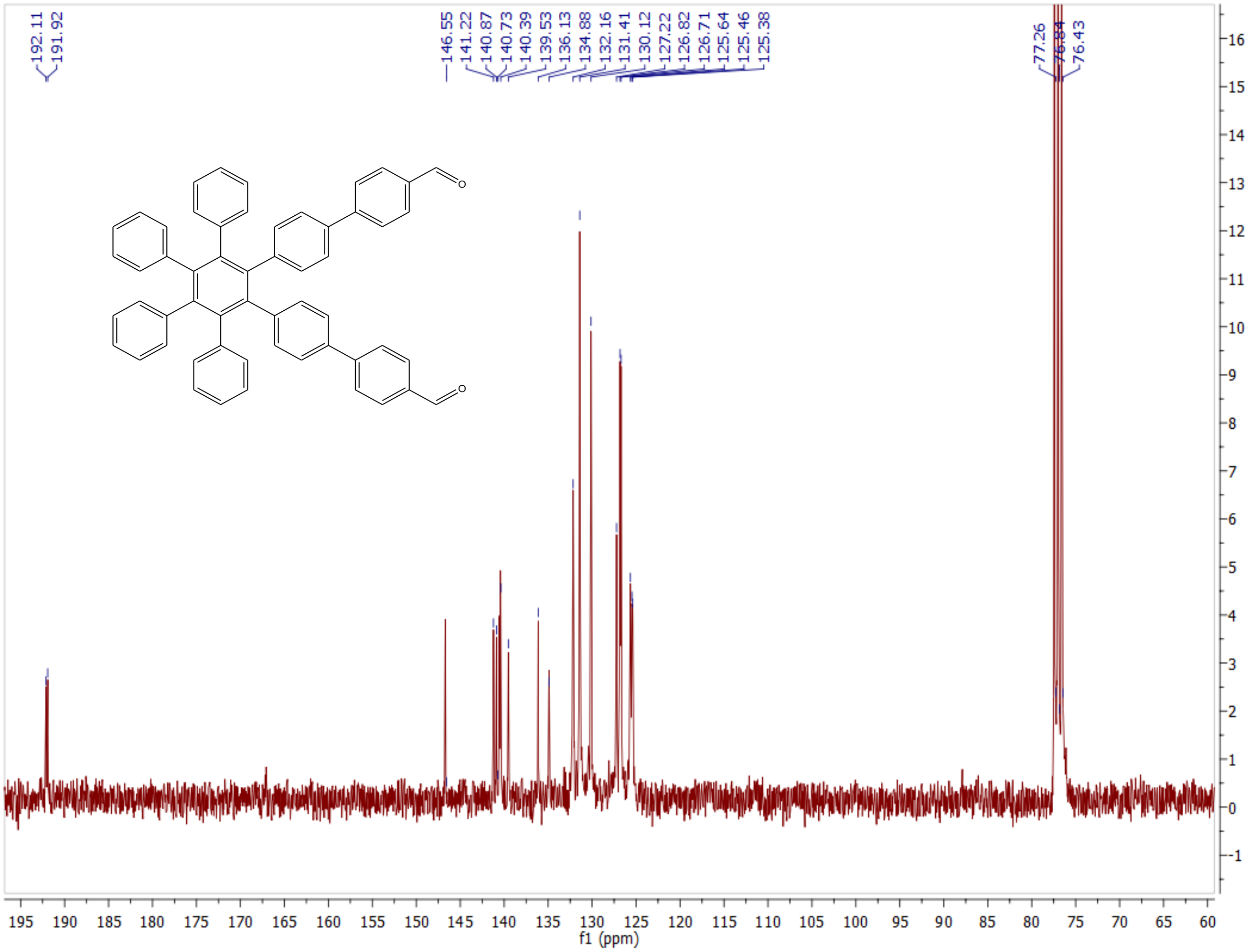

Fig. 40 ^{13}C NMR spectrum of derivative **5** in $CDCl_3$

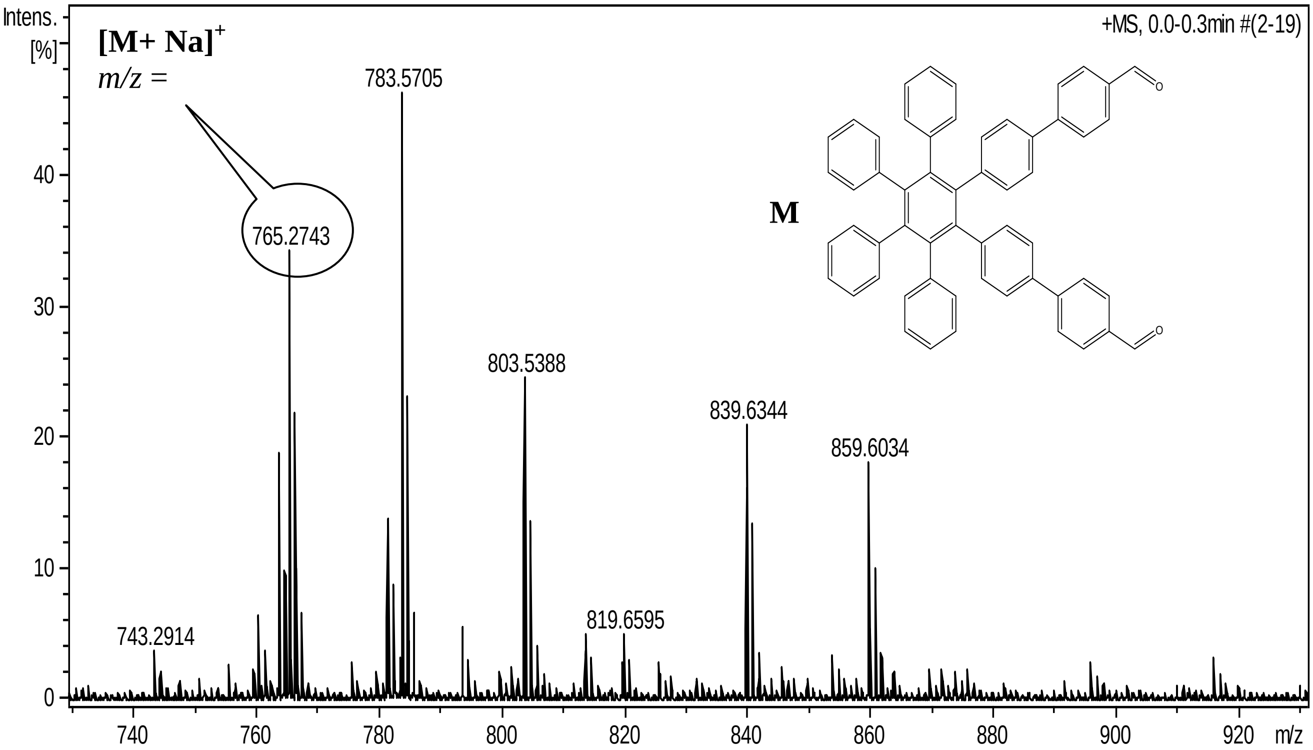

Fig. 41 Mass spectrum of derivative **5.**

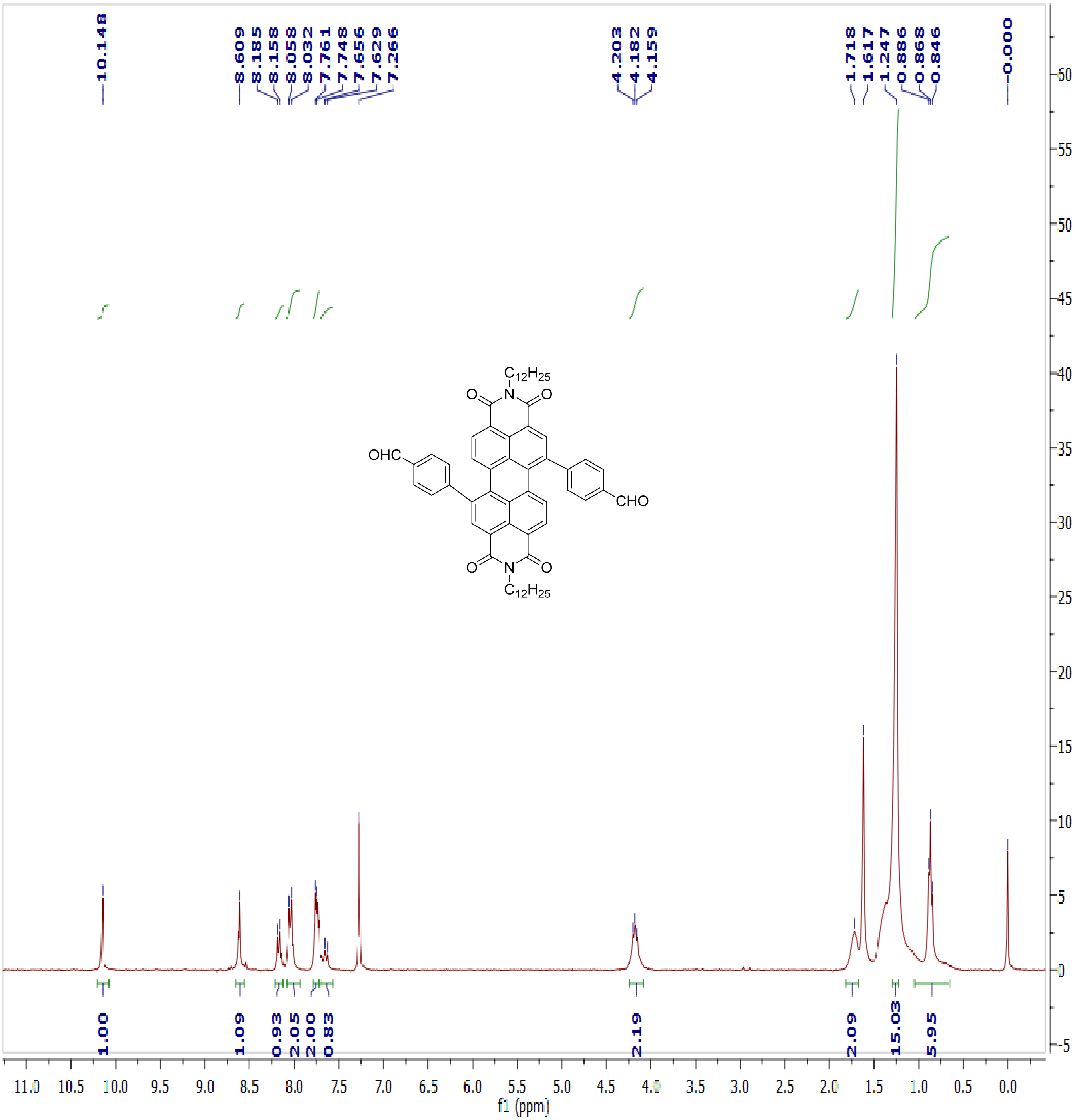

Fig. S42 ^{1}H NMR spectrum of compound **7** in $CDCl_3$.

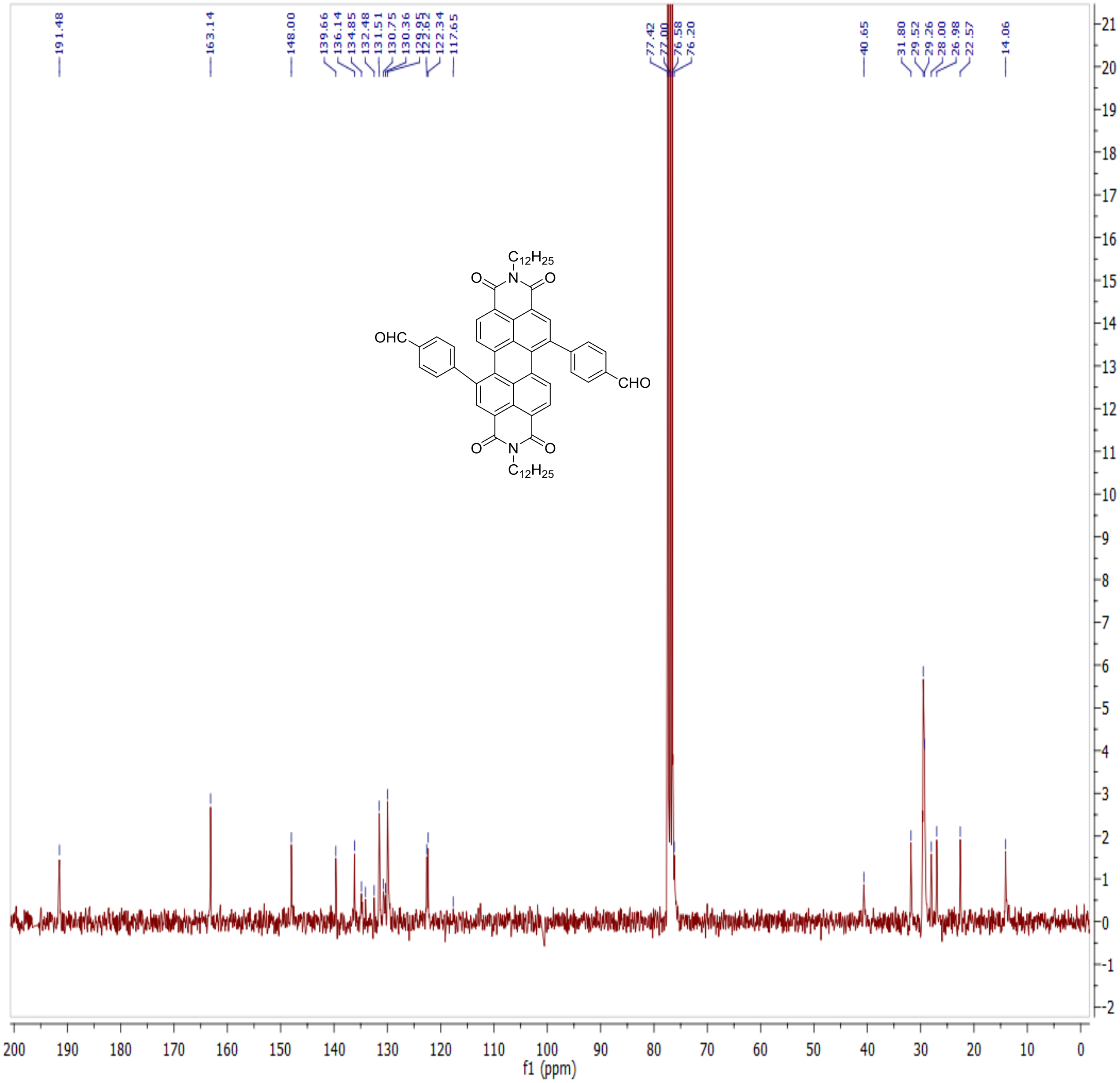

Fig. S43 ^{13}C NMR spectrum of compound **7** in $CDCl_3$.

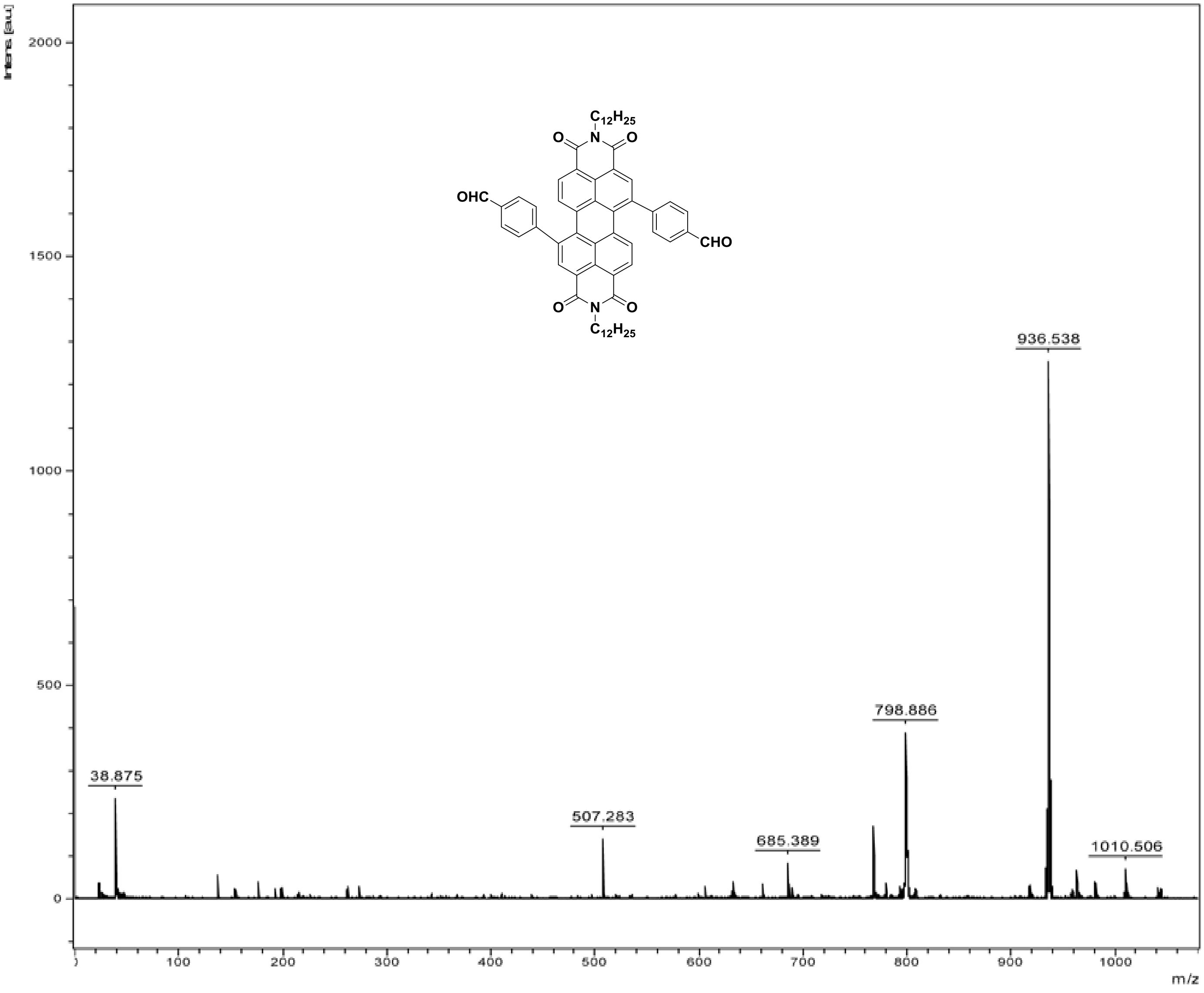

Fig. S44 Mass spectrum of compound **7**.